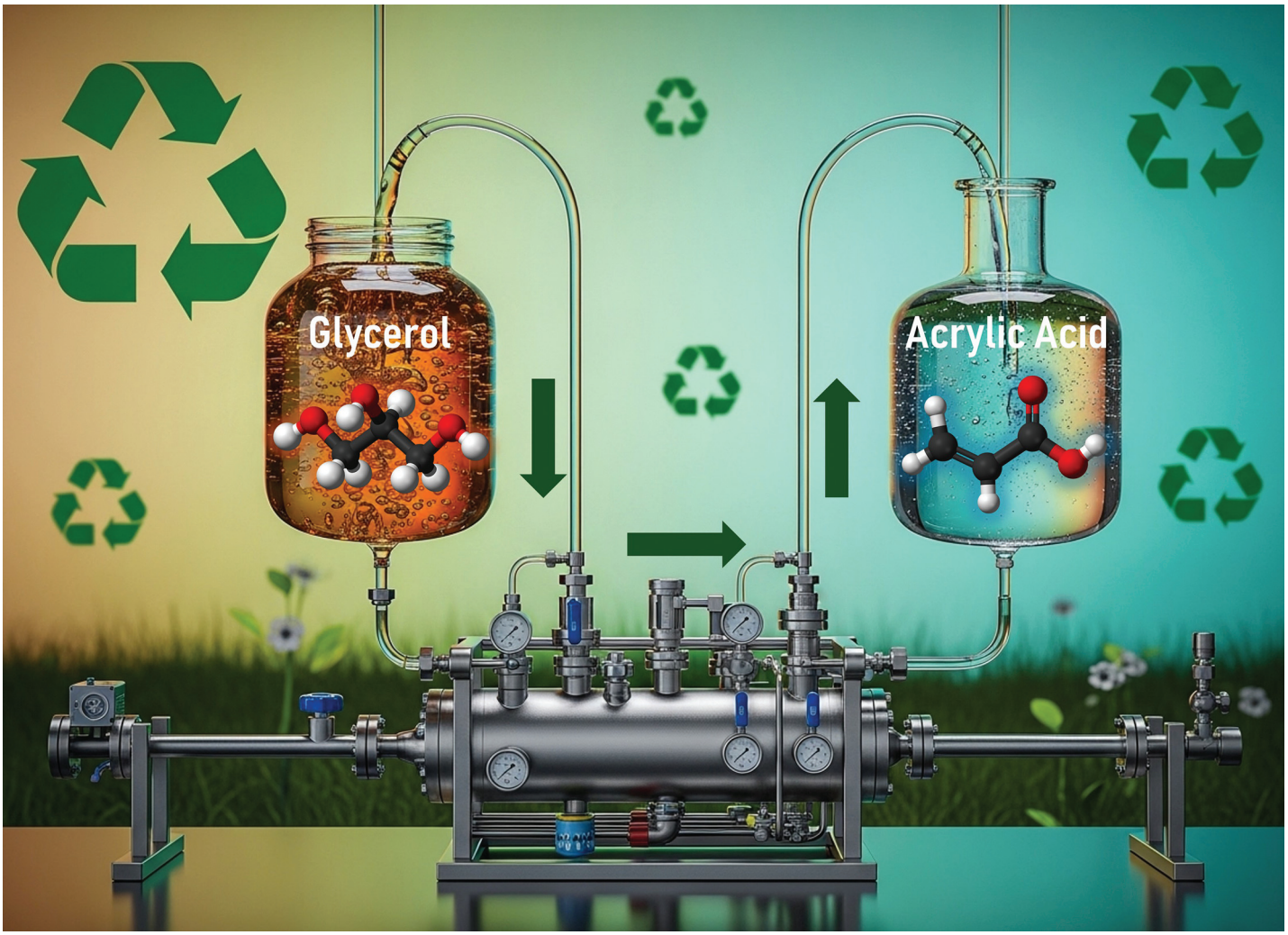

Showcasing research from Dr. Carmine D'Agostino's laboratory, Department of Chemical Engineering, The University of Manchester, Manchester, United Kingdom.

Techno-economic assessment of bio-based routes for acrylic acid production

This study evaluates the economic viability of producing acrylic acid from renewable glycerol feedstock as an alternative to conventional fossil fuel-based processes. Four production pathways were assessed at industrial scale, comparing three glycerol-based routes *via* allyl alcohol, lactic acid, and acrolein intermediates against the conventional propylene-based process. The glycerol-to-acrylic acid *via* acrolein pathway emerged as the most promising bio-based alternative, demonstrating profitability, lowest capital investment, and superior environmental performance. These findings support the transition toward sustainable chemical production using biodiesel industry waste streams.

Image reproduced by permission of Yash Bansod and Carmine D'Agostino from *Green Chem.*, 2025, **27**, 10612.

Artwork generated with AI and created by Yash Bansod.

As featured in:

See Vincenzo Spallina, Carmine D'Agostino *et al.*, *Green Chem.*, 2025, **27**, 10612.

ROYAL SOCIETY OF CHEMISTRY

rsc.li/greenchem

Registered charity number: 207890

Green Chemistry

PAPER

View Article Online
View Journal | View Issue

Cite this: *Green Chem.*, 2025, **27**, 10612

Techno-economic assessment of bio-based routes for acrylic acid production†

Yash Bansod,[a] Mostafa Jafari,[b] Prashant Pawanipagar,[a] Kamran Ghasemzadeh,[a,c] Vincenzo Spallina *[a] and Carmine D'Agostino *[a,d]

This work evaluates the techno-economic performance of biobased and conventional routes for producing acrylic acid, a key industrial chemical. Four pathways were assessed at 79.2 ktonnes per year production capacity: three glycerol-based routes (*via* allyl alcohol, lactic acid, and acrolein) and the conventional propylene-based route. Key performance indicators related to acrylic acid yield, energy consumption, CO_2 emissions, and raw material usage, as well as capital expenditure, OPEX, profitability, and payback period were compared. Among the glycerol-based routes, the lactic acid intermediate route had the highest carbon conversion efficiency (80%), followed by the alcohol intermediate route (74%). From an environmental perspective, propylene-based and glycerol-based allyl alcohol intermediate routes had the highest direct CO_2 emissions, whereas the glycerol-based acrolein intermediate route had the lowest CO_2 emissions. Regarding costs, the glycerol-based allyl alcohol route had the highest capital investment ($247.7 million), while the acrolein route required the lowest ($173.6 million). Moreover, the glycerol-based acrolein intermediate route was the only profitable pathway ($21.6 million annually) but with a commercially unattractive payback period of 11.6 years. Sensitivity analyses revealed that the propylene-based route was the most vulnerable to changes in raw material prices, whereas the acrolein intermediate route was the most resilient to price fluctuations in raw material and utilities, maintaining profitability until a 25% increase in raw material prices. The findings suggest that the renewable glycerol-based acrolein intermediate route can be a promising alternative to conventional acrylic acid production, supporting a transition towards a more sustainable bio-based chemical industry.

Received 9th April 2025,
Accepted 7th July 2025

DOI: 10.1039/d5gc01769f

rsc.li/greenchem

Green foundation

1. This study provides the first comprehensive techno-economic assessment of biobased acrylic acid production from glycerol (a biodiesel industry by-product), establishing economic viability metrics that complement our previous environmental assessment and supporting the transition from fossil-based to renewable feedstocks.
2. Our quantitative achievement shows that the glycerol-to-acrylic acid *via* the acrolein pathway achieves 1.32 kg CO_2 per kg acrylic acid (lowest direct emissions) and $173.6 million capital investment (lowest among biobased routes), and maintains profitability despite raw material price fluctuations up to 25% – demonstrating economic resilience while using renewable feedstock.
3. This work could be made greener through process intensification targeting catalyst optimization, advanced separation technologies, and integration of renewable energy sources, which would enhance carbon efficiency, reduce the 11.6-year payback period, and further minimize environmental footprint.

1. Introduction

Among biofuels, biodiesel production has been growing around the world since the last decade.[1] As a result of rising oil prices, energy security priorities, and the need for low-carbon fuels, global biodiesel production reached over 56 billion litres in 2022 and is projected to increase by 66.9 billion litres by 2032.[2]

Renewable feedstock such as vegetable oils and animal fats, composed primarily of triglycerides and free fatty acids, undergo transesterification reaction with short-chain alcohols (primarily methanol, though ethanol, butanol, and 2-propanol

[a]Department of Chemical Engineering, University of Manchester, Manchester, M13 9PL, UK. E-mail: vincenzo.spallina@manchester.ac.uk, carmine.dagostino@manchester.ac.uk
[b]School of Chemical Engineering, College of Engineering, University of Tehran, Tehran, Iran
[c]School of Engineering, University of Edinburgh, Edinburgh, EH9 3JL, UK
[d]Dipartimento di Ingegneria Civile, Chimica, Ambientale e dei Materiali (DICAM), Alma Mater Studiorum – Università di Bologna, Via Terracini, 28, 40131 Bologna, Italy

†Electronic supplementary information (ESI) available. See DOI: https://doi.org/10.1039/d5gc01769f

are also used depending on regional availability and market conditions) to produce biodiesel and glycerol.[3–5] Approximately, 100 kg of crude glycerol is produced as a by-product per tonne of biodiesel produced from the transesterification reaction.[6] The global production of crude glycerol is substantial, particularly low-quality crude glycerol from second-generation biodiesel production that uses waste-based feedstock.[7,8] Hence, valorisation of crude glycerol has attracted much interest among researchers such as solketal,[9] glycerol carbonate,[10] lactic acid,[11] acrolein,[12] acrylic acid,[13] 2,3-butanediol,[14] syngas (by reforming),[15] aromatics-rich hydrocarbons,[16] fuel bio-additives,[17] methanol,[18] esters and ethers.[19]

Acrylic acid is an essential chemical building block used globally in a wide array of industries including plastics, coatings, adhesives, elastomers, and personal care products.[20,21] The worldwide production capacity of acrylic acid was over 8.12 million tons in 2022 with a market value of $14.6 billion,[22] with demand growing 3–5% annually.[23] The predominant industrial process to produce acrylic acid starts with fossil fuel-derived propylene as a feedstock. In the first step, propylene is oxidized to acrolein over bismuth molybdate-based catalysts in the presence of a steam–air mixture and later into acrylic acid.[24] In this two-step route, propylene has an overall conversion of over 95% and around 80–90% acrylic acid yield is achieved.

Abubakar *et al.*[25] reported that biochemical conversion routes are the most promising to produce acrylic acid from glycerol when considered from an environmental perspective as they have lower energy requirements, whereas, from an economic perspective, thermocatalytic conversion routes are the most promising as these routes provide higher acrylic acid yields. A different promising bio-based route to acrylic acid utilizes allyl alcohol as an intermediate derived from glycerol (Fig. 1). Glycerol can be converted to allyl alcohol through several methodologies including gas phase transfer hydrogenation,[26] rhenium complex-catalysed deoxydehydration,[27] and formic acid-mediated non-catalytic deoxydehydration.[28] This route first converts glycerol to allyl alcohol *via* deoxydehydration using formic acid as a reaction mediator, as opposed to a heterogeneous catalyst, followed by catalytic oxidation of allyl alcohol to obtain the target acrylic acid product.

The lactic acid intermediate pathway is another interesting route for converting glycerol into acrylic acid. This multi-step process first requires transforming the glycerol into either dihydroxyacetone or pyruvaldehyde.[29] The intermediate can then be converted to lactic acid, followed by acid-catalysed dehydration of lactic acid to yield the target acrylic acid product.[30,31] While this three-reaction sequential transformation is more complex and requires three catalytic processes, the pathway benefits from simultaneously generating the commercially valuable chemicals dihydroxyacetone and lactic acid along with the desired acrylic acid.

Brobbey *et al.*[32] performed a techno-economic assessment study of three biobased acrylic acid production pathways using sugarcane A-molasses (liquid residue left after the first stage of sugar manufacturing process) as the renewable feedstock. The study compared process routes utilizing lactic acid, 3-hydroxypropionic acid, or glycerol intermediates based on economic and sustainability criteria and reported that the route having lactic acid as an intermediate was superior compared to other pathways but with a limited acrylic acid yield, lower than 40% for all three processes. Okoro *et al.*[33] explored and compared two bio-based pathways, including lactic acid fermentation, followed by chemical conversion to acrylic acid as well as pyrolysis of apple pomace waste to ultimately yield propylene for subsequent acrylic acid production. Bhagwat *et al.*[34] specifically analysed pathways using corn stover feedstock to initially generate the 3-hydroxypropionic (HP) acid intermediate before acrylic acid conversion. Their analysis compared different microbial fermentation approaches to produce the 3-HP intermediate. In another work, Sandid *et al.*[35] carried out a techno-economic assessment study of two acrylic acid production processes using glycerol and propylene as the feedstock.

While previous techno-economic and sustainability studies have tentatively explored bio-based acrylic acid production, a comprehensive study comparing routes derived from the same feedstock (glycerol) using a consistent methodology and set of assumptions is not available in the literature. Our previous work focused on the environmental sustainability evaluation of these pathways through a cradle-to-gate life cycle assessment (LCA), revealing significant variations in global warming potential, water footprint, acidification, and other environ-

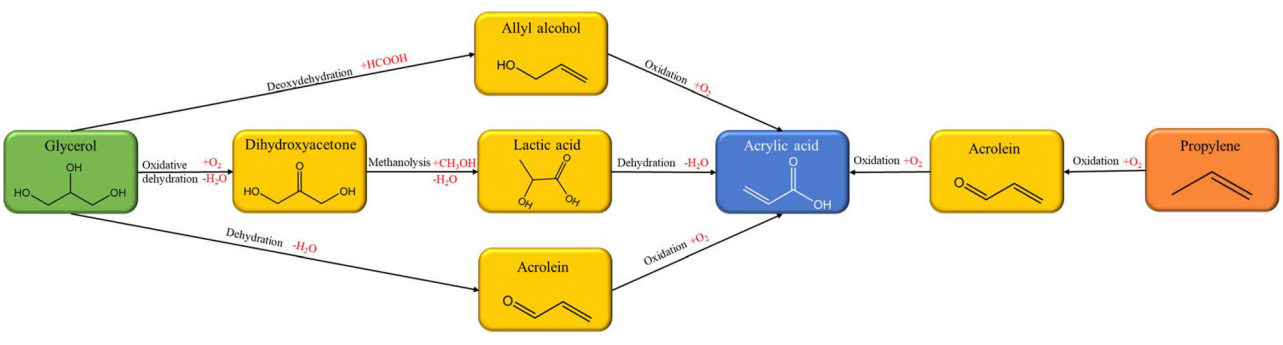

Fig. 1 Different pathways to produce acrylic acid from glycerol and propylene.

mental impacts among different routes.[36] That study demonstrated that glycerol-based processes exhibited higher environmental impacts compared to conventional propylene-based production when using epichlorohydrin-derived glycerol, but showed substantial improvements when using purified crude glycerol from the biodiesel industry.

This work aims to cover the existing gap in process engineering and techno-economic studies by assessing the economic viability of the same four process routes: three glycerol-based pathways (*via* allyl alcohol, lactic acid, and acrolein) in comparison with the conventional propylene oxidation route. The study provides an in-depth simulation of mass and energy flow, equipment sizing and capital investment estimation, operating cost analysis, and market pricing potential. Furthermore, we integrate heat recovery strategies and perform comprehensive sensitivity analyses to identify key economic drivers and barriers to implementation. Together with our previous LCA findings, this techno-economic assessment creates a complete sustainability framework that enables informed decision-making, regarding which glycerol valorisation pathway offers the most promising balance of environmental and economic performance. The goal of this research work is to evaluate whether renewable feedstock-based production routes can serve as viable alternatives to replace current fossil fuel-based acrylic acid production, and to identify specific process intensification opportunities that could bridge remaining economic gaps.

2. Methodology

This techno-economic assessment builds upon our previous environmental sustainability evaluation[36] while introducing several key methodological differences and extensions. While the LCA study focused on environmental impact metrics, this work prioritizes economic indicators, capital cost estimation, and profitability analysis. The same four production routes are examined: (1) glycerol to acrylic acid *via* allyl alcohol (G-AA (*via* ALY)), (2) glycerol to acrylic acid *via* lactic acid (G-AA (*via* LAC)), (3) glycerol to acrylic acid *via* acrolein (G-AA (*via* ACR)), and (4) conventional propylene to acrylic acid *via* acrolein (P-AA (*via* ACR)).

Key methodological extensions in this work include detailed equipment sizing and costing using factorial method approaches, heat integration analysis to identify energy recovery potential, and comprehensive capital expenditure (CAPEX) and operating expenditure (OPEX) estimation. The economic assessment is further enhanced through profitability analysis including payback period calculation and extensive sensitivity analysis for raw material, utility, and product pricing fluctuations. These additional economic dimensions provide crucial insights into commercial viability that complement our previous environmental findings.

2.1. Process design

Process simulation is carried out in Aspen Plus V12.1. For glycerol-based processes having allyl alcohol and acrolein as intermediates, the NRTL-HOC package within the Aspen software was used for performing the thermodynamic calculations,[37] whereas for the P-AA (*via* ACR) and G-AA (*via* LAC) processes, the UNIQUAC package was used.[38] The NRTL-HOC method was specifically selected for acrolein-containing processes because these systems involve multiple carboxylic acids (acrylic acid as the main product, and acetic acid and propionic acid as the by-products) that exhibit strong hydrogen bonding and dimerization in the vapor phase. The Hayden–O'Connell equation of state component accounts for these vapor-phase association effects, while the NRTL equation handles the non-ideal liquid-phase behaviour. This combination is essential for accurate vapor–liquid equilibrium predictions in carboxylic acid-containing systems, which deviate significantly from ideal gas behaviour due to molecular association.[39] In the G-AA (*via* LAC) process, the thermodynamic calculations associated with the purification processes of dihydroxyacetone were performed using the SOLIDS package within the Aspen software. The four processes were simulated assuming operations 7920 hours per year and generating *ca.* 10 000 kg h^{-1} acrylic acid (>99.5 wt%).[40] This production capacity was selected based on practical industrial scale considerations and to enable a direct comparison with our previous LCA study. The feasibility of this production scale was verified against available feedstock supply: the annual UK output of FAME biodiesel is 1.6 million tonnes,[41] which results in the production of approximately 160 thousand tonnes of crude glycerol. This translates to about 20 tonnes per hour of crude glycerol, which is more than sufficient to meet the amount of acrylic acid production required in this study.

2.2. Assumptions

The main assumptions made to compute the mass and energy balances are outlined here. The sizing methodology and cost evaluation approach used for the major components are provided here. The costs were then scaled to match the current equipment sizes and updated using the chemical engineering cost index for 2023.

2.2.1. Reactors. Fixed bed catalytic reactors were modelled as plug flow reactors (PFRs) and their size was changed to achieve the maximum conversion of the reactants. The ratio of length to diameter (L/D) was set to 5 for optimal performance, which is typical for industrial applications.[42] Moreover, the maximum diameter was limited to 5 m, while the maximum length was 15 m based on standard equipment sizing considerations and ease of transport to facility locations during installation.[43] For highly exothermic reactions such as allyl alcohol oxidation, acrolein oxidation and propylene oxidation, a multi-tubular reactor was utilised with tubes of 2 inch diameter. For multi-tubular reactor design, the number of tubes was determined using a systematic approach based on Gas Hourly Space Velocity (GHSV). The total gas flow rate entering the reactor was first calculated and converted to volumetric units. A GHSV of 1000 h^{-1} was applied to determine the required catalyst volume by dividing the gas flow rate by the

GHSV.[39] A 25% operational margin was incorporated to account for operational flexibility and feed condition variations. The volume of each individual tube was calculated using $V = \pi \times (d/2)^2 \times L$, where d represents the internal diameter (*i.e.* two inches) and L is the tube length. The total number of tubes was then determined by dividing the total required catalyst volume (including margin) by the volume per tube. For semi-batch reactors, the volume of the reactor was calculated using the volume of the reactants per unit time and factoring 25% extra volume for mixing and headspace allowance.[44] The PFR was assumed to be a vertical pressure vessel for thickness calculation and cost estimation purposes. The reactions, reactants, products, and catalysts used, along with the kinetic rate type used, rate constants, activation energy, and adsorption terms are extensively discussed and detailed in the ESI† for each case.

2.2.2. Heat exchangers and turbomachines. Heat exchangers were modelled as shell and tube and assumed to have no pressure drop. Compressors, turbines, and blowers were assumed to have an isentropic efficiency of 75% and a mechanical efficiency of 100%. Pumps were assumed to have a pump efficiency of 75% and the cost of explosion-proof motors driving each of the pumps was also considered in the economic analysis.

2.2.3. Separation columns. The mass and energy balance calculation of the distillation and absorber columns was done using the RadFrac method in Aspen Plus. For the liquid–liquid extractor, an extract unit within the Aspen was used and as this tool cannot perform the sizing of a liquid–liquid extractor due to the complexity of the equipment, the size of the extractor was estimated using the ratios of total inlet flow rates and the sizing data available for the absorber.

2.2.4. Raw materials. The composition of crude glycerol from the biodiesel industry can vary widely depending upon the type of catalyst used (base catalysts: NaOH and KOH; acid catalysts like HCl and H_2SO_4), the process efficiency, impurities contained within the feedstock, and the efficiency of recovery of biodiesel and solvents from the reaction mixture.[7] While crude glycerol requires purification before catalytic conversion to high-value chemicals, this study focuses solely on the conversion process of purified glycerol. The purification part of the crude glycerol has not been considered in this study since it would be the same for all glycerol-based processes. For the purposes of this study, adequately purified glycerol was assumed to be functionally equivalent to pure glycerol as a raw material. For the G-AA (*via* ALY) and G-AA (*via* ACR) routes, the glycerol feedstock stream was modelled as 85 wt% pure (or purified) glycerol mixed with 15 wt% water, whereas for the G-AA (*via* LAC) process, the glycerol feedstock was kept as 52.5 wt% in water as per previous studies.[45] It is important to note that when calculating the raw material costs, only the weight percentage of pure glycerol was used to determine the total price, not the entire mixture. Attarbachi *et al.*[7] reported an operating cost of 20.4 USD per ton for the purification of glycerol derived from second-generation biodiesel production. To maintain a conservative approach in this analysis, a unit cost of 200 USD per ton for the 85 wt% purity glycerol feedstocks was assumed. This value is an order of magnitude higher than that reported by Attarbachi *et al.*[7] and falls within the lower bound of the current commercial price range for glycerol of ≥80 wt% purity, which spans from 150 to 650 USD per kg.[46] For the propylene-based process, propylene feedstock was modelled as chemical grade propylene with mole composition of propylene : ethane : propane = 94 : 3 : 3.[47]

2.2.5. Solid processing. Dihydroxyacetone was converted to solid crystals using the crystallizer unit in Aspen Plus. The saturation calculation method used was based on the solubility data of dihydroxyacetone obtained from ref. 48. The solids were filtered in a solid filter, assuming a recovery of 99.9% solids. The DHA crystals were washed in solid washers with acetone and the mixing efficiency of the solid washer was assumed to be 100% with the liquid to solid ratio as 97%. The solid dryer was attached with a blower and was assumed to be operating at a temperature of 50 °C to completely remove the residual washing solvent, *i.e.*, acetone.[49]

2.2.6. Catalysts. Due to the lack of consistent and publicly available data on the specific heterogeneous catalysts used across the various bio-based routes, uniform catalyst assumptions were applied to all processes. All heterogeneous catalysts were assumed to have the same cost and a uniform lifespan of 10 years. Since this study is comparative in nature, focusing on the relative techno-economic performance of different production routes, the same catalyst cost and lifespan assumptions were applied consistently across all processes to ensure valid relative comparisons.

2.3. Heat integration

To identify potential energy saving opportunities, pinch analysis methodology was employed using process stream data extracted from Aspen Plus simulations. The analysis considered heating and cooling streams from all separation units, heat exchangers, and reactors across the four processes. The minimum energy requirements for each process were determined using a minimum temperature approach of 10 °C for general heat exchange and 5 °C for streams requiring refrigeration. The Grand Composite Curves (GCC) were constructed to visualize the heat recovery potential and determine the pinch point temperature for each process. The details of the heat integration data are presented in section 3 of the ESI.† Through this systematic approach, the minimum hot and cold utility requirements were established, enabling the calculation of potential energy savings compared to the base case designs.

2.4. Economic analysis

The calculation of the total capital expenditure (CAPEX) was done using the factorial method. The costs associated with the capital costs and operating costs along with their calculation method are given in section 1 (Tables S1 and S2) of the ESI.†[42] For equipment and installation costs, the purchased cost for each equipment was based on the year 2010. The Chemical Engineering Plant Cost Index (CEPCI) with a value of 821 (2024) was used to adjust the equipment costs for inflation.[50]

Table 1 Prices of raw materials and utilities used in this study

Raw material	Value	Ref.
Glycerol	204 USD per tonne	7 and 52
Formic acid	430 USD per tonne	53
Acetone	1280 USD per tonne	54
Methanol	570 USD per tonne	55
DIPE	2050 USD per tonne	56
Toluene	976 USD per tonne	57
Propylene	1120 USD per tonne	58
Feed water	0.72 USD per tonne	59
Acrylic acid	2500 USD per tonne	60
Utilities	**Value**	**Ref.**
Power electricity	0.24 USD per kWh	61
Cooling water	0.21 USD per GJ	59
LP steam (P = 1 bar)	1.90 USD per GJ	59
MP steam (P = 8.75 bar)	2.20 USD per GJ	59
HP steam (P = 39.43 bar)	2.50 USD per GJ	59
Fired heat	4.25 USD per GJ	
Refrigerant	2.74 USD per GJ	59

Table 2 Key performance indicators used in this study

Parameter	Unit	Equation
Carbon conversion	%	$\gamma_c = \frac{n_{RE}}{n_{AA}}$
Raw material consumption (RM)	kg kg^{-1}	$RM = \frac{m_{RM}}{m_{AA}}$
Water/steam requirement (WR)	kg kg^{-1}	$WS = \frac{m_{WS}}{m_{AA}}$
Air requirement (AR)	kg kg^{-1}	$AR = \frac{m_{AIR}}{m_{AA}}$
Solvent requirement (SR)	kg kg^{-1}	$SR = \frac{m_{SR}}{m_{AA}}$
Electricity requirement (ER)	kWh kg^{-1}	$ER = \frac{m_{ER}}{m_{AA}}$
Overall energy consumption (OER)	kWh kg^{-1}	$OER = \frac{m_{OER}}{m_{AA}}$
Liquid wastes generated (LW)	kg kg^{-1}	$LW = \frac{m_{LW}}{m_{AA}}$

Moreover, the total fixed capital cost was adjusted by a location factor of 1.21 for UK as the initial calculated fixed capital cost was based on the US Gulf Coast.[51] More details about the types of equipment and their sizing are given in section 1 (Tables S5–S8) in the ESI.† Based on UK, the prices of the raw materials, utilities, and acrylic acid are given in Table 1.

2.5. Key performance indicators

The starting feed (glycerol/propylene) is converted into the desired product (acrylic acid) for each process and require energy in the form of electricity and heat. Additionally, unreacted gaseous feed that does not get converted is then separated and incinerated, contributing to CO_2 emissions to the environment. The key performance indicators (KPIs) used for the process comparison are listed in Table 2. By evaluating these factors, the aim is to conduct a fair assessment of the technical and environmental performance across the processes examined.

2.6. Kinetic models

The summary of the reactions, reactants, products, and catalysts used in this study is given in individual processes in the process description. More detailed information about the kinetic rate type used, rate constants, activation energy, and adsorption terms for each reaction can be found in section 2 of the ESI.†

2.7. Process description

2.7.1. Glycerol to acrylic acid *via* allyl alcohol

Unit one: glycerol to allyl alcohol. Fig. 2 shows the process flow diagram integrating all the unit operations involved in the G-AA (*via* ALY) process. Glycerol and formic acid were mixed at a molar ratio of 1 : 1.8,[28] and the resulting mixture was then introduced into the first reactor (REACTOR-1). The reactor operated at a temperature of 235 °C and formic acid mediated the formation of allyl alcohol. The product stream (S3) con-

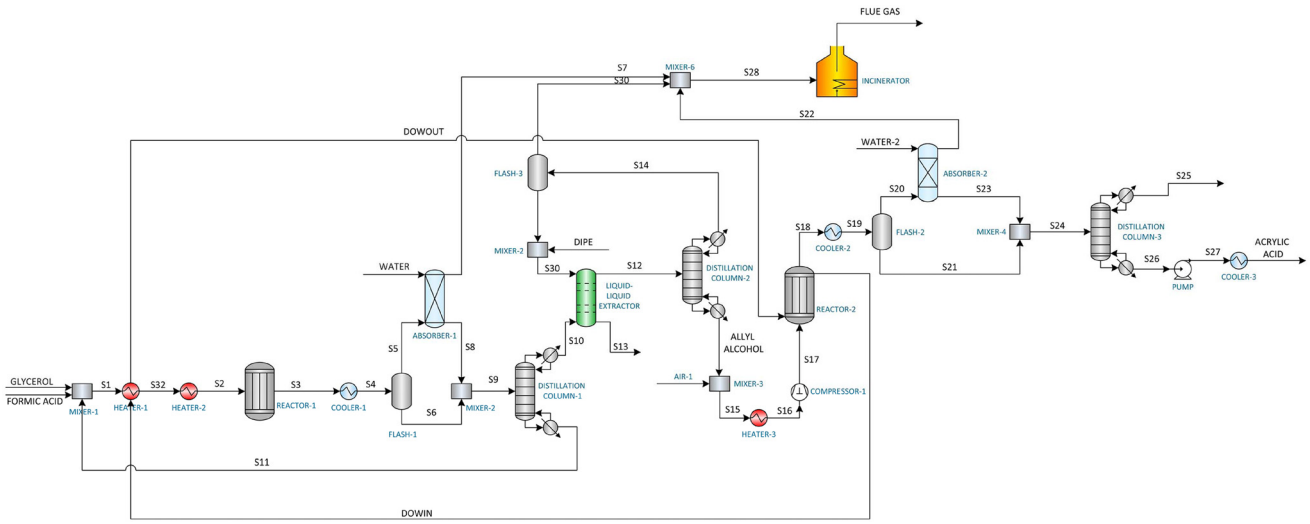

Fig. 2 Process flow diagram for the G-AA (*via* ALY) process.

Table 3 Reaction information for the G-AA (*via* ALY) process

	Reaction no.	Reaction	Yield (%)	Catalyst used	Table in the ESI† showing detailed kinetics
Deoxydehydration of glycerol to allyl alcohol	1	Glycerol + formic acid → allyl alcohol + CO_2 + $2H_2O$	98.0%	Formic acid[a]	—
Oxidation of allyl alcohol to acrylic acid	1	Allyl alcohol + O_2 → acrylic acid + H_2O	76.1%	Molybdenum/ vanadium/tungsten mixed oxide	Table S9†
	2	Allyl alcohol + $0.5O_2$ → acrolein + H_2O	14.3%		
	3	Allyl alcohol + O_2 → 1.5 acetic acid	8.0%		
	4	Allyl alcohol + $4O_2$ → $3CO_2$ + $3H_2O$	7.8%		
	5	Allyl alcohol + $2.5O_2$ → 3CO + $3H_2O$	4.7%		

[a] Formic acid was used as a mediator.

taining allyl alcohol, unreacted reactants, and undesired products was cooled down to 25 °C using a heat exchanger (COOLER-1) to prevent the formation of any side products. Table 3 shows detailed reaction information of the G-AA (*via* ALY) process including the reactions and yields of the products. The non-condensable gas component (CO_x) of the product stream was removed in the flash drum (FLASH-1). The gas phase of the top stream (S5) exiting the flash drum consisted of some allyl alcohol vapours and was recovered in the absorber (ABSORBER-1) by generating an aqueous solution of allyl alcohol (S8) using water. In the next step, the liquid phase stream (S6) from the flash drum and the aqueous allyl alcohol solution were sent to the distillation column (DISTILLATION COLUMN-1) to recover the unreacted formic acid. The bottom product of the distillation column containing formic acid (31%) and water (69%) was recycled back to the reactor. The top distillate (of DISTILLATION COLUMN-1) consisted of allyl alcohol (23%) and the rest was water. Distillation cannot be used to separate allyl alcohol from water as these compounds tend to form an azeotrope at atmospheric pressure.[62] Hence, the liquid–liquid extraction method was used to facilitate effective separation of allyl alcohol from water. An organic solvent DIPE was used to extract allyl alcohol from water due to its immiscibility with water and affinity for allyl alcohol. The allyl alcohol–water stream (S10) was flowed into the liquid–liquid extractor (LIQUID–LIQUID EXTRACTOR) unit. The extract (S12) of the liquid–liquid extractor containing DIPE (92%) was sent to the second distillation column (DISTILLATION COLUMN-2) operating for DIPE solvent recovery. The residual non-condensable gases from the DIPE-rich distillate (S14) were removed in a flash drum (FLASH-3) operating at 30 °C and the bottom liquid stream (69% DIPE and the rest water) from the flash was recycled back to the liquid–liquid extractor after blending it with fresh makeup DIPE.

Unit two: allyl alcohol to acrylic acid. The pure allyl alcohol stream (ALLYL-AL) from the second distillation column was mixed with excess air to keep its concentration well below the lower flammability limit of 2.5%.[63] The mixture was then heated at 230 °C and sent to the oxidation reactor (REACTOR-2) operating at 1 bar where allyl alcohol was converted to acrylic acid. The heat generated by the reactor was used to heat the S1 stream from 78.9 °C to 164.3 °C using DOWTHERM-A. Following this, any non-condensable gases (CO_x) from the output steam (S18) from the reactor were removed in the flash drum (FLASH-2) operating at 85 °C. However, the gas stream (S19) of the flash drum also contained a few acrylic acid vapours which were recovered using the absorber (ABSORBER-2). An aqueous acrylic acid solution (S20) was generated from the acrylic acid vapour by flowing water into the absorber. Both streams were mixed and sent to the purification column operating at reduced pressure of 0.2 bar to achieve acrylic acid at the required 99.5% purity level. Acrylic acid is highly susceptible to thermal polymerization when exposed to high temperatures. Distilling under reduced pressure decreases the boiling point, allowing separation at lower temperatures, thereby minimizing the risk of unwanted polymerization and thermal decomposition during the process.[64] Waste gases (S31, S7 and S21) from the flash drum (FLASH-3) and absorber (ABSORBER-1 and ABSORBER-2) were sent to the incinerator to remove any toxic organic vapours and excess air was supplied to the incinerator for complete combustion. The energy released by the incinerator was used to heat the S32 stream from 164.3 °C to 234.9 °C and the S15 stream from 8 °C to 106 °C using DOWTHERM-A. More details in terms of composition, flow rate and pressure of the process shown in Fig. 2 are provided in the ESI† (section 3.1).

2.7.2. Glycerol to acrylic acid *via* lactic acid

Unit one: glycerol to dihydroxyacetone. Fig. 3 shows the flow diagram for the G-AA (*via* LAC) process, depicting the interconnected unit operations for the overall process. Glycerol was fed into a batch reactor system *via* semi-continuous feeding over a duration of six hours, with continuous flow of air as a source of oxygen. The products generated – dihydroxyacetone (DHA) and glyceraldehyde – were flowed to a flash drum. Table 4 shows the complete reaction information of the G-AA (*via* LAC) process including the reactions and yields of the products. The unreacted air component of the product mixture was removed using a flash drum (FLASH-1) operating at atmospheric pressure. The liquid phase stream (S4) from the flash drum bottom was fed into a distillation column (DISTILLATION COLUMN-1) to separate DHA from the product mixture. Subsequently, DHA (88.8 wt%) was sent to a solid crystallizer to produce pure solid DHA crystals, which were then filtered in a solid filter (S-FILTER). Solubility data of DHA for the crystalli-

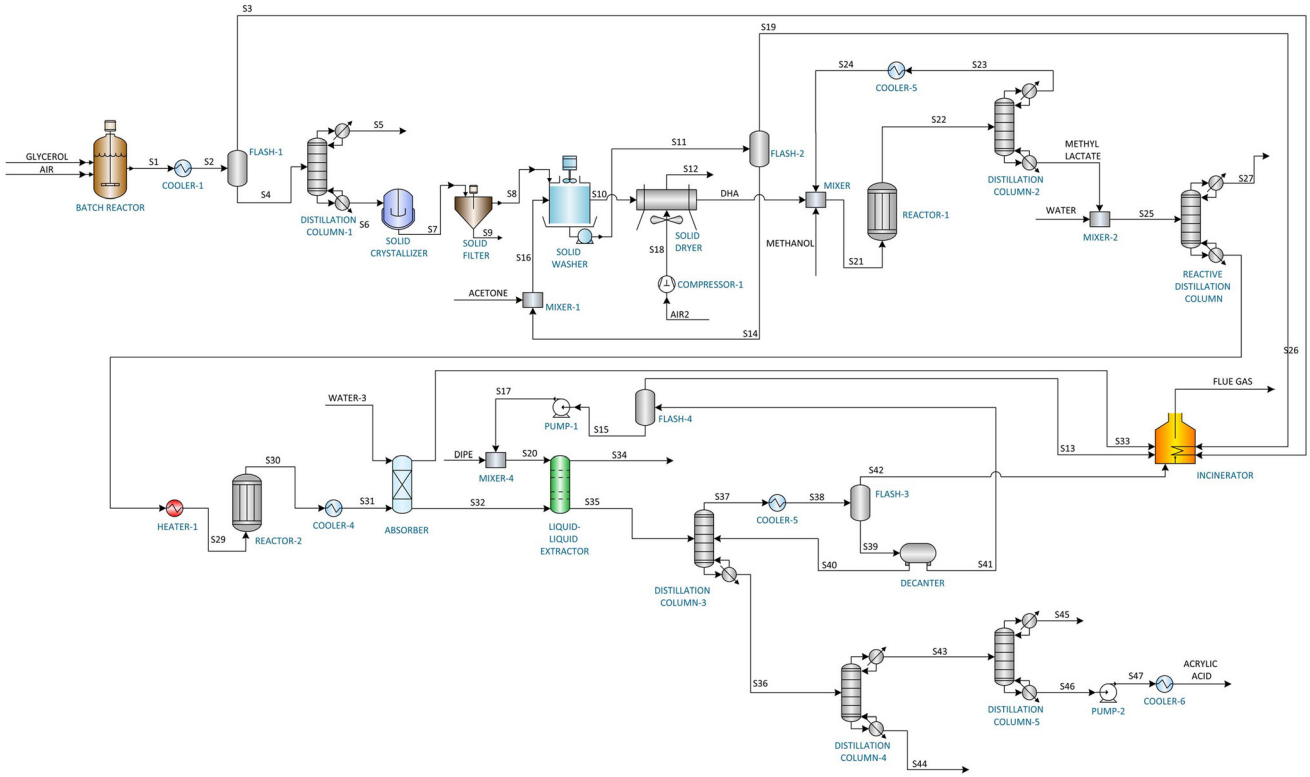

Fig. 3 Process flow diagram for the G-AA (*via* LAC) process.

Table 4 Reaction information for the G-AA (*via* LAC) process

	Reaction no.	Reaction	Conversion/ yield (%)	Catalyst used	Tables in the ESI† showing detailed kinetics
Oxidative dehydration of glycerol to DHA	1	Glycerol + $0.5O_2$ → dihydroxyacetone + H_2O	87.0%	Carbon-supported bismuth	Table S10†
	2	Glycerol + 0.5 O_2 → glyceraldehyde + H_2O	13.0%		
Conversion of DHA to methyl lactate	1	Dihydroxyacetone → pyruvaldehyde + H_2O	99.9%	H-USY zeolite	Table S11†
	2	Pyruvaldehyde + methanol → methyl lactate	2.6%		
	3	Pyruvaldehyde + H_2O → glyceraldehyde	97.4%		
Hydrolysis of methyl lactate to lactic acid	1	Methyl lactate + H_2O ↔ lactic acid + methanol	99.99%	Acidic cation-exchange resin (D001)	Table S12†
Dehydration of lactic acid to acrylic acid	1	Lactic acid → acrylic acid + H_2O	95.54%	K-Exchanged ZSM-5	Table S13†
	2	Lactic acid → acetaldehyde + H_2O + CO_2	4.48%		

zation unit of DHA were taken from ref. 48. The solid DHA crystals went through washing with acetone in a solid washer and drying in a dryer using air at 50 °C to remove residual acetone from DHA solids.

Unit two: dihydroxyacetone to lactic acid. In the next section, the DHA crystals were dissolved with methanol in a 1 : 2.5 molar ratio and fed to the second reactor operating at 120 °C to produce methyl lactate.[45] The product stream (S22) from the second reactor was flowed into the distillation column to recover the unreacted methanol and separate the methyl lactate product. The recovered methanol stream (99.9 wt%) was recycled back to the mixer where DHA was being dissolved with methanol. Methyl lactate was then mixed with water to create a solution having 10 wt% methyl lactate and 90 wt% water.[65] The solution was then fed to the reactive distillation column for the hydrolysis reaction for the conversion of methyl lactate into lactic acid. Following this, the lactic acid was flowed to the third reactor after heating it at 360 °C.[66]

Unit three: lactic acid to acrylic acid. Dehydration of lactic acid to acrylic acid was carried out in the third reactor. The product mixture from the third reactor containing acrylic acid, acetaldehyde, and CO_2 along with the unreacted reactants was then cooled down in a heat exchanger and sent to the absorber to remove the non-condensable gases and to generate an aqueous solution of acrylic acid. The aqueous acrylic acid solution stream (S32) was flowed into the liquid–liquid extraction unit to extract acrylic acid from the water using DIPE solvent. The extract stream (S35), comprising primarily of acrylic acid

and DIPE solvent, was flowed into the solvent recovery column operating at 0.3 bar. The DIPE-rich distillate was flashed out into a flash drum to eliminate any remaining non-condensable gases. The bottom liquid stream of the flash drum was flowed to the decanter and the water separated from the decanter was returned to the solvent recovery column as an external reflux. The second liquid stream from the decanter containing residual DIPE was flashed out again in the flash drum and recycled back to the liquid–liquid extractor with makeup DIPE. The acrylic acid rich bottom product from the solvent recovery column was flowed through another distillation column for glyceraldehyde removal, followed by water removal in the final distillation column for the required purity level of acrylic acid.

More details in terms of composition, flow rate and pressure of the process shown in Fig. 3 are provided in the ESI† (section 3.2).

2.7.3. Glycerol to acrylic acid *via* acrolein

Unit one: glycerol to acrolein. The glycerol to acrylic acid *via* acrolein process simulation was based on the process proposed by Sandid *et al.*,[35] with operating conditions taken from Dimian *et al.*[37] and with slight modifications in the operating conditions to optimize the yield of the final acrylic acid product. Fig. 4 outlines the sequence of unit operations included in the process. Initially, glycerol, steam, and air were preheated to 372 °C and fed into the first reactor, operating at 3.9 bar, where glycerol was converted to acrolein. Table 5 shows the reaction information of the G-AA (*via* ACR) process including the reactions and yields of the products. The product stream from the first reactor was then passed through a distillation column to remove the by-products such as hydroxyacetone and propionic acid. The acrolein-rich distillate stream (S8) was mixed with excess air to keep its concentration well below the lower flammability limit of 2.8%.[67] This mixed stream was then pressurized to 2.4 bar and heated to 350 °C before entering the second oxidation reactor.

Unit two: acrolein to acrylic acid. The oxidation reactor converted acrolein into acrylic acid and the exiting product stream (S14) from the reactor was cooled immediately to prevent further by-product formation. Non-condensable gases (CO_2) were separated from the product stream using a flash drum.

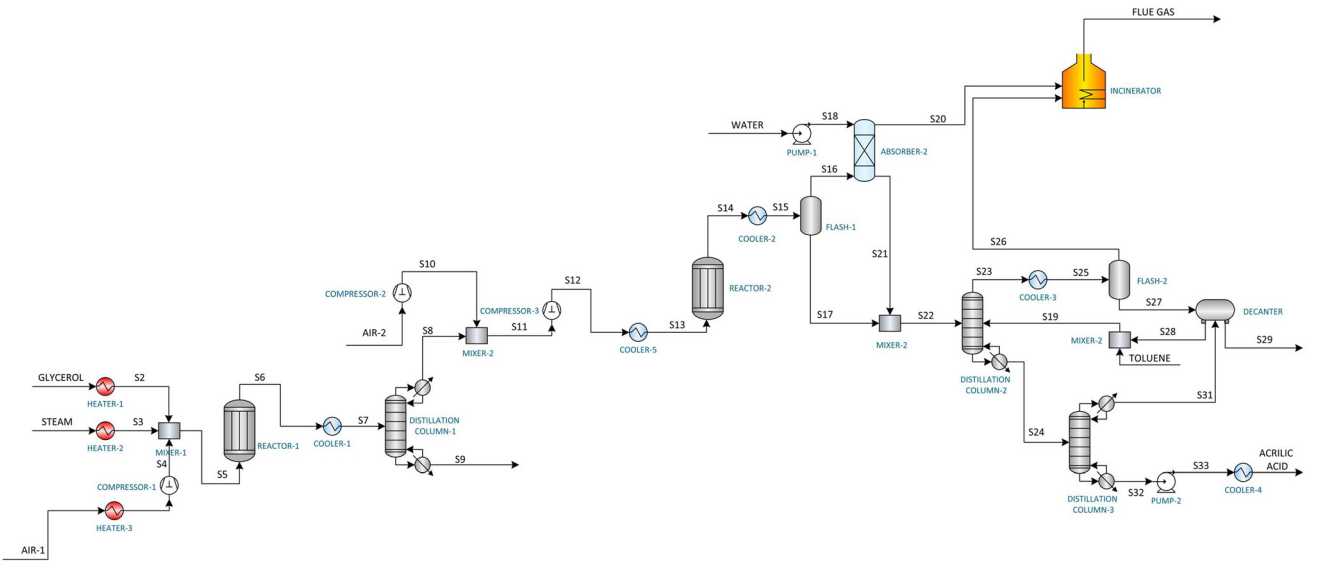

Fig. 4 Process flow diagram for the G-AA (*via* ACR) process.

Table 5 Reaction information for the G-AA (*via* ACR) process

	Reaction no.	Reaction	Conversion/ yield (%)	Catalyst used	Tables in the ESI† showing detailed kinetics
Dehydration of glycerol to acrolein	1	Glycerol → acrolein + $2H_2O$	81.6%	Alumina-supported silicotungstic acid	Table S14†
	2	Glycerol → acetol + H_2O	9.2%		
	3	Glycerol → acetaldehyde + CO + H_2O + H_2	0.3%		
	4	Acrolein + H_2O → propionic acid	3.8%		
	5	Acetol → acetone + $0.5O_2$	4.0%		
Oxidation of acrolein to acrylic acid	1	Acrolein + $0.5O_2$ → acrylic acid	84.9%	Molybdenum/ vanadium mixed oxide	Table S15†
	2	Acrolein + $3.5O_2$ → $3CO_2$ + $2H_2O$	9.0%		
	3	Acrolein + $2O_2$ → 3CO + $2H_2O$	6.3%		

However, the top stream of the flash drum (S16) also contained residual vapours of acrylic acid along with non-condensable gases. To recover the acrylic acid vapours, the top stream from the flash drum was sent to an absorber with water flowing from the top, and an aqueous acrylic acid solution was recovered at the bottom of the absorber. The bottom liquid phase stream (S17) from the flash drum and the aqueous acrylic acid solution (S21) were mixed and sent to a distillation column for further purification. Azeotropic distillation was employed due to the presence of water–acetic acid and water–acrylic acid azeotropes, with toluene as an entrainer. The vapor distillate (S23) from the distillation column, containing mostly water and toluene, was cooled and flashed in a flash drum. The bottom liquid phase product (S27) of the flash drum was fed into a decanter to separate and recycle the toluene back to the distillation column as an external reflux. The bottom product (S24) of the distillation column was sent to a final distillation column for further purification of the acrylic acid product to the required purity level. The distillate from the final distillation column consists mostly of toluene and water; therefore, it was sent to a decanter for toluene–water separation. The vapor streams (S20 and S26) from the absorber and flash drum were combusted in an incinerator, resulting in a flue gas.

More details in terms of composition, flow rate and pressure of the process shown in Fig. 4 are provided in the ESI† (section 3.3).

2.7.4. Propylene to acrylic acid *via* acrolein

Unit one: propylene to acrylic acid. The propylene to acrylic acid *via* the acrolein process was based on the simulation provided by Sandid *et al.*[43] with slight modifications in the operating conditions to achieve the target amount and purity of acrylic acid. Fig. 5 depicts the unit step operations for the process. Propylene, air, and steam were mixed at a molar ratio of 1 : 10.7 : 4 and heated to 366 °C before being fed to the first fixed bed reactor.[68] This reactor was a multi-tubular packed-bed reactor consisting of 1750 tubes of 2 inch diameter. In this reactor, propylene was oxidised to form acrolein. Table 6 shows the reaction information of the P-AA (*via* ACR) process including the reactions and yields of the products. The product stream containing acrolein from the first reactor was pressurized to 2.4 bar and heated to a temperature of 350 °C. This product stream was mixed with excess air to keep its concentration well below the lower flammability limit of 2.8%.[67] Subsequently, this mixed stream entered the second multi-tubular packed-bed reactor, where the acrolein underwent oxidation to form acrylic acid. The product stream exiting the second reactor was sent to an absorber unit, where the cooling water stream reduced the temperature of the incoming vapours, producing an aqueous acrylic acid solution and allowing the non-condensable gases to escape from the top of the column.[68] The top stream leaving the absorber contained some residual acrylic acid vapours along with the non-condensable gases, which were then flashed out in the flash drum. These streams (S10 and S12) were subsequently mixed and fed into the liquid–liquid extractor.

Unit two: acrylic acid purification. The extraction of acrylic acid from an aqueous solution was carried out *via* a liquid–liquid extraction process using DIPE as the solvent. The extract (S14), comprising mainly acrylic acid and DIPE solvents, was then sent to the solvent recovery column operating at 0.3 bar to produce a DIPE-rich distillate. This distillate was flashed in the flash drum to remove any non-condensable gases, and the bottom liquid stream was sent to the decanter. The water separated from the DIPE solvent in the decanter was recycled back to the solvent recovery distillation column as an external reflux. Since the raffinate phase from the extractor still con-

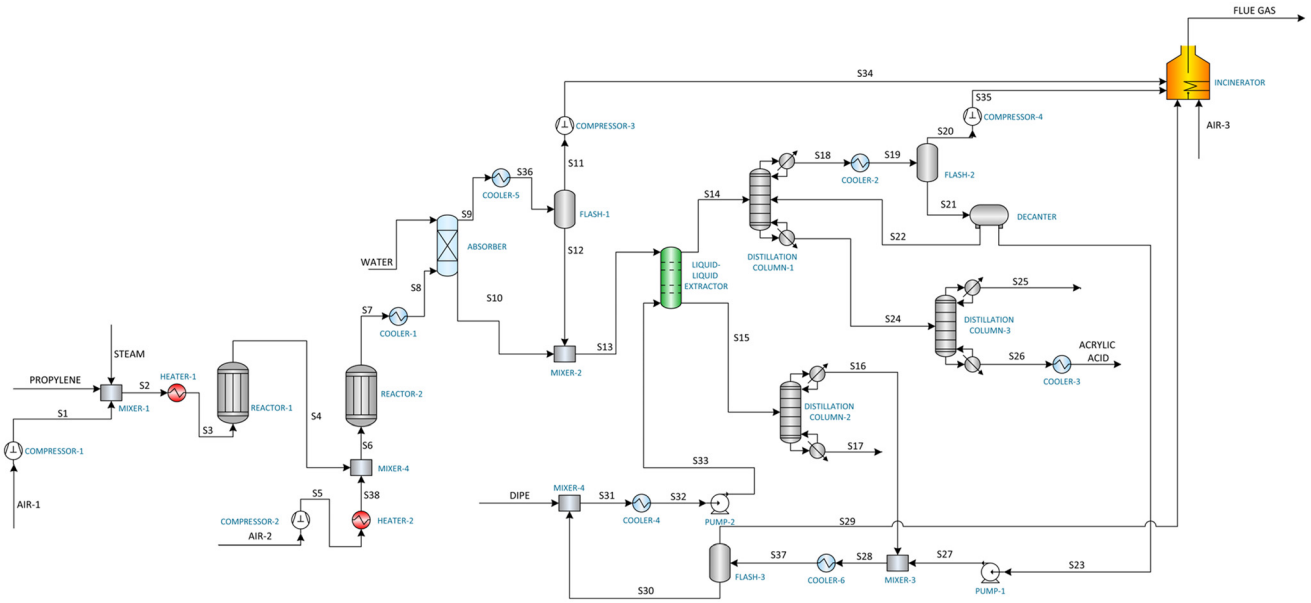

Fig. 5 Process flow diagram for the P-AA (*via* ACR) process.

Table 6 Reaction information for the P-AA (*via* ACR) process

	Reaction no.	Reaction	Yield (%)	Catalyst used	Tables in the ESI† showing detailed kinetics
Oxidation of propylene to acrolein	1	Propene + O_2 → acrolein + H_2O	70.8%	Bismuth molybdate	Table S16†
	2	Acrolein + $0.5O_2$ → acrylic acid	7.2%		
	3	Acrylic acid + $3O_2$ → $3CO_2$ + $2H_2O$	0.0%		
	4	2 propene + $9O_2$ → $6CO_2$ + $6H_2O$	0.0%		
	5	Propene + O_2 → acetaldehyde + formaldehyde	1.6%		
	6	2 acetaldehyde + O_2 → 2 acetic acid	1.5%		
	7	Propene + $3O_2$ → 3CO + $3H_2O$	0.0%		
	8	2 acrolein + $3O_2$ → 4 formaldehyde + $2CO_2$	3.7%		
	9	Acetic acid + $2O_2$ → $2CO_2$ + $2H_2O$	0.9%		
	10	Acetaldehyde + $2.5O_2$ → $2CO_2$ + $2H_2O$	2.5%		
Oxidation of acrolein to acrylic acid	1	Acrolein + $0.5O_2$ → acrylic acid	85.0%	Molybdenum/ vanadium mixed oxide	Table S17†
	2	Acrolein + $3.5O_2$ → $3CO_2$ + $2H_2O$	26.9%		
	3	Acrolein + $2O_2$ → 3CO + $2H_2O$	18.4%		

tained some remaining DIPE solvent, it was fed into a second distillation column for purification. The DIPE-rich liquid distillate from this column was mixed with the DIPE solvent from the decanter and recycled back to the liquid–liquid extractor, with makeup DIPE added as necessary. The bottom liquid product from the solvent recovery column, containing mostly water and acrylic acid, was sent to a final vacuum distillation column operating at 0.1 bar to achieve the required purity level. Finally, waste streams from the flash drums (S34, S29, and S35) were incinerated in an incinerator, with excess air fed to ensure complete combustion.

More details in terms of composition, flow rate and pressure of the process shown in Fig. 5 are provided in the ESI† (section 3.4).

3. Results and discussion

3.1. Kinetic model comparison

The simulation results for the four acrylic acid production processes were validated against the literature data, and the results exhibited a maximum deviation of 10% from the reported conversion and selectivity values. Comprehensive details on this comparative analysis are given in Table S18 of the ESI.†

3.2. Technical comparison

The information provided in Table 7 reflects the diverse requirements for each pathway to produce acrylic acid effectively from the selected feedstocks. Considering only the carbon conversion of reactants to the desired product, the reactors of the G-AA (*via* LAC) process appear to be the best performing with the three reactors (BATCH REACTOR, REACTOR-1, and REACTOR-2) providing the products in 86.97%, 97.37%, and 95.16% yields, respectively. Moreover, the operating conditions for the three reactors in the G-AA (*via* LAC) process were relatively moderate compared to other processes, suggesting that the energy requirement can be lower. However, for non-commercial processes, these results would require further validation while the processes are upscaled and confirmed in terms of separating the desired products from the by-products, in addition to the carbon conversion efficiency.

Table 8 provides a detailed overview of the separation equipment and their operating conditions for the various processes investigated to produce acrylic acid from different feedstocks. The stage requirements, reboiler types, and recovery percentages vary depending on the specific separation challenges posed by the product mixtures and the desired purity levels. The G-AA (*via* LAC) process involved intermediate steps like the formation of dihydroxyacetone, methyl lactate, and lactic acid, and hence, required additional distillation columns for purification of these intermediates prior to flowing them to the next reactor. The G-AA (*via* LAC) process employed twice the number of distillation columns compared to other processes, reflecting the increased complexity associated with the presence of multiple intermediates in a process. Liquid–liquid extraction was used in the G-AA (*via* ALY), G-AA (*via* LAC) and P-AA (*via* ACR) routes to overcome the challenge posed by the formation of azeotropic mixtures, whereas the G-AA (*via* ACR) route used azeotropic distillation for this purpose. It is crucial to note that an increased number of distillation columns does not necessarily translate to a proportional increase in utility requirements or capital investment. These factors are influenced by various other parameters, such as the specific products to be separated, volumetric flow rates, operating pressures, and other process-specific considerations.

Fig. 6 shows the grant composite curves (GCC) of the four acrylic acid production routes. The hot utility is required to be at a temperature higher than 240 °C, 365 °C, 505 °C and 371 °C for the allyl alcohol, lactic acid, acrolein and conventional propylene routes, respectively. Table 9 presents the heat integration results for all processes, highlighting significant variations in utility requirements. The G-AA (*via* ALY) process showed minimum utility requirements of 60.0 MW for hot utility and 81.8 MW for cold utility. The actual heat and cold demands before heat integration were substantially higher at

Table 7 Information about the reactor dimensions, operating conditions and the desired products

Process	Reactor name	Diameter (m) and the number of tubes	Length (m)	Volume of the reactor (m^3)	Temperature (°C)	Pressure (bar)	Desired products from the reactor	Yield of the product
G-AA (*via* ALY)	REACTOR-1	2.16	10.82	—	235	1	Allyl alcohol	98.0%
	REACTOR-2	0.049 (2100)	4.82	—	230	2.3	Acrylic acid	76.1%
G-AA (*via* LAC)	BATCH REACTOR	—	—	168.84	50	1	Dihydroxyacetone	87.0%
	REACTOR-1	1.36	6.80	—	120	2	Methyl lactate	97.4%
	REACTOR-2	0.95	4.75	—	360	1	Acrylic acid	95.5%
G-AA (*via* ACR)	REACTOR-1	1.16	5.80	—	375	3.9	Acrolein	81.6%
	REACTOR-2	0.049 (2250)	3.12	—	350	2.4	Acrylic acid	84.9%
P-AA (*via* ACR)	REACTOR-1	0.049 (1750)	2.9	—	360	3.67	Acrolein	70.8%
	REACTOR-2	0.049 (2250)	3.12	—	350	2.4	Acrylic acid	85.0%

Table 8 Details about the column, operating conditions, and the desired separation products

Process	Equipment	Condenser	Reboiler	Number of stages	Feed stage	Desired separation products	Initial mole fraction	Final mole fraction	% Recovery
G-AA (*via* ALY)	ABSORBER-1	—	—	10	—	Allyl alcohol	0.008	0.046	80.48
	DISTILLATION COLUMN-1	Partial	Kettle	18	9	Formic acid	0.200	0.309	99.99
	LIQUID-LIQUID EXTRACTOR	—	—	10	—	Allyl alcohol	0.234	0.135	99.99
	DISTILLATION COLUMN-2	Partial	Kettle	10	5	Allyl alcohol	0.135	0.965	99.99
	ABSORBER-2	—	—	6	—	Acrylic acid	0.001	0.187	99.33
	DISTILLATION COLUMN-3	Partial	Kettle	17	8	Acrylic acid	0.431	0.994	97.06
G-AA (*via* LAC)	DISTILLATION COLUMN-1	Total	Kettle	6	3	DHA	0.142	0.888	99.99
	DISTILLATION COLUMN-2	Total	Kettle	14	8	Methyl lactate	0.269	0.487	99.99
	REACTIVE DISTILLATION COLUMN	Total	Kettle	44	8	Lactic acid to methyl lactate	0.088	0.905	99.99
	ABSORBER	—	—	10	—	Acrylic acid	0.085	0.083	99.99
	LIQUID-LIQUID EXTRACTOR	—	—	8	—	Acrylic acid	0.083	0.197	99.99
	DISTILLATION COLUMN-3	—	Kettle	20	10	Acrylic acid	0.197	0.277	99.99
	DISTILLATION COLUMN-4	Total	Kettle	8	4	Acrylic acid	0.277	0.277	99.52
	DISTILLATION COLUMN-5	Total	Kettle	12	6	Acrylic acid	0.284	0.285	99.30
G-AA (*via* ACR)	ABSORBER	—	—	4	—	Acrylic acid	0.002	0.673	62.65
	DISTILLATION COLUMN-1	Partial	Kettle	8	4	Acrolein	0.087	0.568	99.99
	DISTILLATION COLUMN-2	—	Kettle	12	6	Acrylic acid	0.634	0.973	91.29
	DISTILLATION COLUMN-3	Total	Kettle	14	7	Acrylic acid	0.973	0.985	89.48
P-AA (*via* ACR)	ABSORBER	—	—	10	—	Acrylic acid	0.021	0.136	99.99
	LIQUID-LIQUID EXTRACTOR	—	—	8	—	Acrylic acid	0.086	0.164	99.90
	DISTILLATION COLUMN-1	—	Kettle	20	10	Acrylic acid	0.164	0.351	99.88
	DISTILLATION COLUMN-2	Partial	Kettle	4	2	DIPE	0.004	0.616	83.64
	DISTILLATION COLUMN-3	Total	Kettle	50	25	Acrylic acid	0.351	0.994	99.58

125.4 MW and 122.9 MW, respectively, indicating significant potential for heat recovery. This high utility requirement of the allyl alcohol route would be attributed to the large amount of feed volumes to be treated by the first and second distillation columns, and hence, the greater energy required by the reboilers. In contrast, the G-AA (*via* ACR) process demonstrated

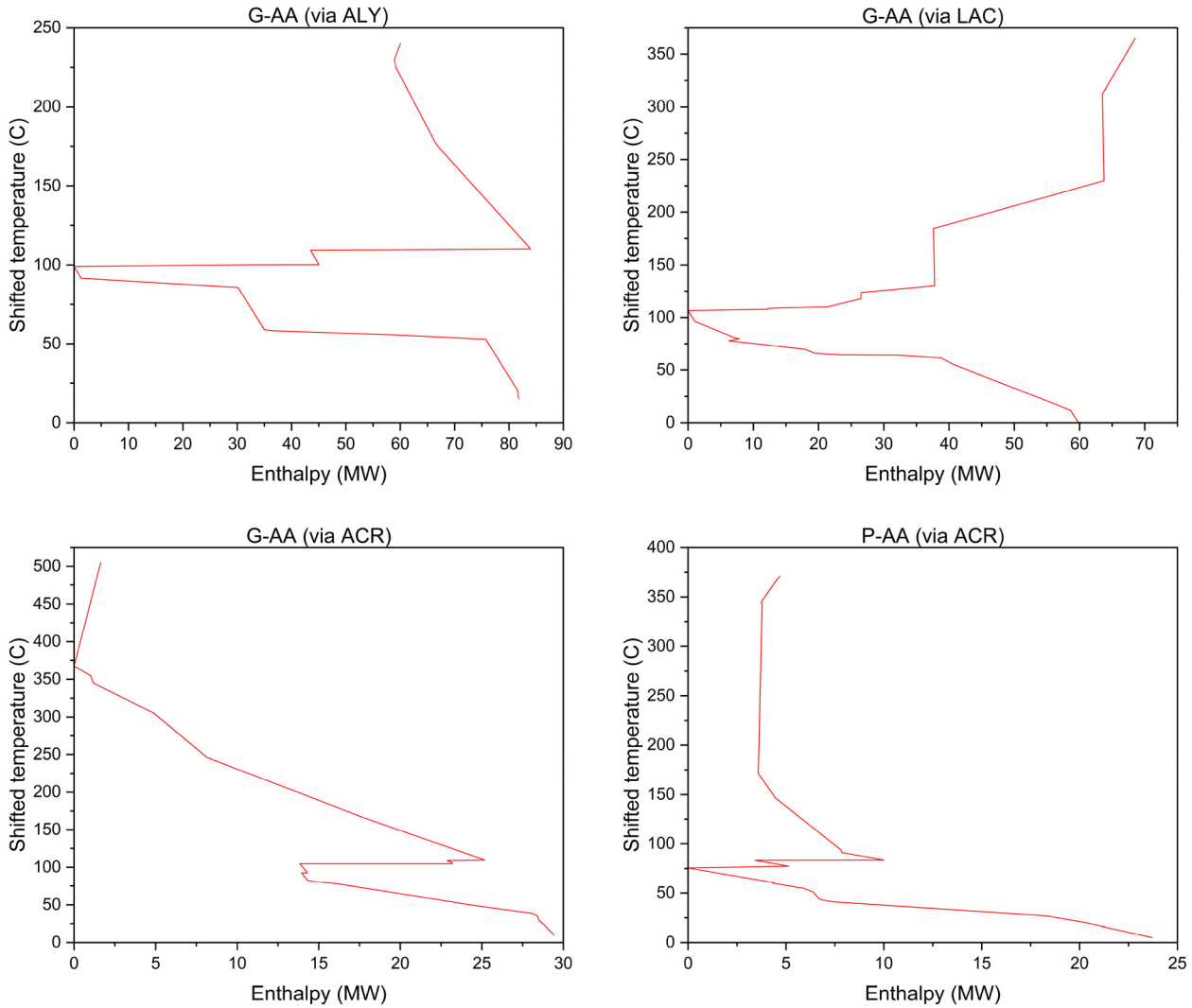

Fig. 6 Grant composite curves for the four acrylic acid production processes.

Table 9 Heat integration results for the four acrylic acid production processes

	G-AA (*via* ALY)	G-AA (*via* LAC)	G-AA (*via* ACR)	P-AA (*via* ACR)
Minimum hot utility (MW)	60.0	68.5	1.6	4.7
Minimum cold utility (MW)	81.8	59.9	29.4	23.7
Actual heat demand (MW)	125.4	118.4	35.9	28.0
Actual cold demand (MW)	122.9	116.0	67.8	46.5
Pinch temperature (°C)	99.1	106.6	367.4	75.5

remarkably lower minimum utility requirements, with only 1.6 MW for hot utility and 29.4 MW for cold utility. This process had the highest pinch temperature at 367.4 °C, corresponding to the high-temperature reaction conditions in the acrolein formation step. The actual heat and cold demands were 35.9 MW and 67.8 MW, respectively, indicating substantial potential for heat recovery through process integration. The G-AA (*via* LAC) process exhibited the highest minimum utility requirements among all routes, requiring 68.5 MW for hot utility and 59.9 MW for cold utility. The actual heat and cold demands (118.4 MW and 116.0 MW, respectively) were also on a relatively higher end. This can be explained by the involvement of several reaction steps to obtain the target acrylic acid as well as the presence of several energy-intensive unit operations, including multiple distillation columns, reactive distillation, and solid–liquid separation processes.

The conventional P-AA (*via* ACR) process also showed relatively low minimum utility requirements of 4.7 MW for hot utility and 23.7 MW for cold utility. The actual heat and cold demands (28.0 MW and 46.5 MW, respectively) were interestingly the lowest demand for both hot and cold utilities among all the processes examined. This is because both the oxidation of propylene to acrolein and dehydration of glycerol to acrolein occur in a gas-phase reaction; however, since propylene is already in the gas phase, it does not need extra energy for

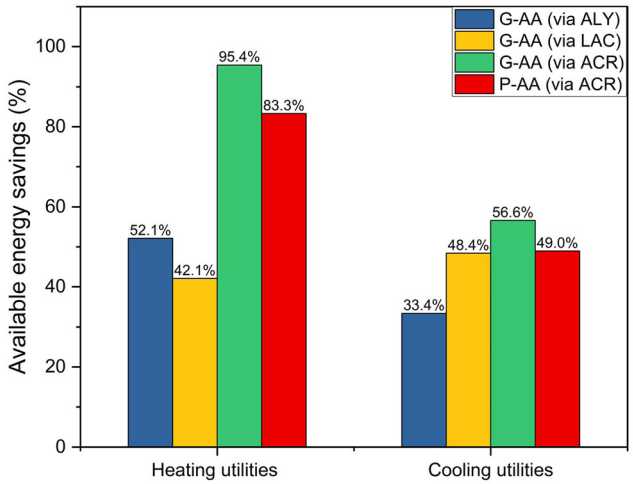

Fig. 7 Comparison of the available energy saving across the four processes.

vaporisation, which is required in the case of glycerol. It is important to note that while the conventional propylene-based route may have lower utility requirements, it relies on fossil fuel-derived feedstocks.

Overall, the implementation of heat integration could result significant energy savings across all processes, as shown in Fig. 7. The G-AA (*via* ACR) process achieved the highest reduction in heating utilities at 95.4%, followed by P-AA (*via* ACR) at 83.3%. The G-AA (*via* ALY) and G-AA (*via* LAC) processes showed more moderate but still substantial heating utility reductions of 52.1% and 42.1%, respectively. The pathways incorporating acrolein oxidation to acrylic acid demonstrated superior heat energy savings, attributed to the highly exothermic nature of this reaction step, which provides valuable opportunities for steam generation. For cooling utilities, all processes demonstrated significant savings ranging from 43.4% to 60.2%. The G-AA (*via* ACR) process achieved the highest cooling utility reduction at 56.6%, while the G-AA (*via* LAC) and P-AA (*via* ACR) processes showed savings of 48.4% and 49.0%, respectively. These results demonstrate that implementing heat integration strategies could substantially improve the energy efficiency of all processes, particularly for the acrolein and allyl alcohol intermediate routes.

Fig. 8 shows a comparison of KPIs (as listed in Table 2) across processes considered in this study. The G-AA (*via* LAC) process had the highest carbon conversion efficiency with a value of 80% closely followed by the G-AA (*via* ALY) process (74%), whereas P-AA (*via* ACR) had the lowest value (63%). The raw material consumption per unit kg of acrylic acid produced was the highest for the G-AA (*via* ACR) process, followed by the G-AA (*via* ALY), G-AA (*via* LAC), and P-AA (*via* ACR) processes. Since the yields of products from the two reactors (81.7% and 84.9%) in the G-AA (*via* ACR) process were comparatively lower than those from the other glycerol-based processes as well as the recovery of AA from the third distillation column was low, more amount of starting feed was required to produce an amount equal to 10 000 kg of acrylic acid. In terms of air consumption, the G-AA (*via* ALY) process had the highest demand per unit kg of acrylic acid, followed by the G-AA (*via* ACR) and conventional P-AA (*via* ACR) routes. This high air requirement of three processes was to maintain the concentrations of flammable reactants well below their lower flammability limits along with air required by the waste incineration involved. The G-AA (*via* LAC) route emerges on the top for the process of

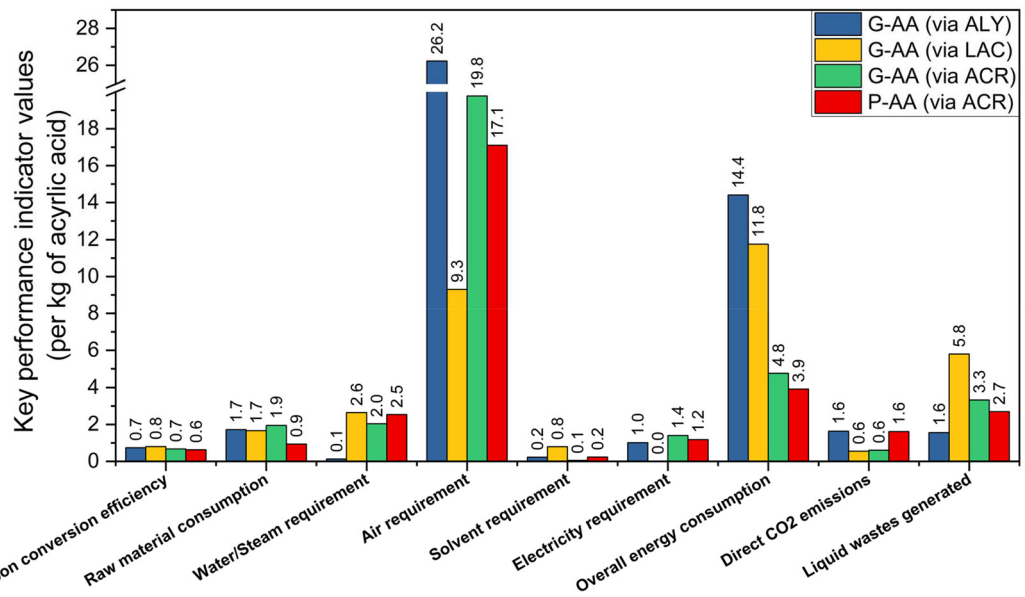

Fig. 8 Process performance indicators per kg of acrylic acid produced by the four acrylic acid production pathways. The RM, WS, AR, SR, and LW values are in kg kg^{-1} units, whereas the ER and OER values are in kWh kg^{-1} units.

water consumption as it requires a substantial amount of water by the hydrolysis reaction occurring in the reactive distillation column as well as due to the water needed by the absorber. Moreover, the P-AA (*via* ACR) route was on the second for the consumption of process water as water was required by the first and second reactors and also by the absorber. In terms of make-up solvent consumption, the G-AA (*via* ALY) and G-AA (*via* LAC) processes demonstrated higher solvent requirements compared to the G-AA (*via* ACR) process, which can be explained by the use of liquid–liquid extraction units in these processes, which utilised solvents like DIPE for the separation and purification of acrylic acid from aqueous streams. The G-AA (*via* ACR) and P-AA (*via* ACR) processes had higher electricity usage due to the usage of compressors to pressurize the reactant streams before flowing them into the reactor. Moreover, the G-AA (*via* LAC) process had a solid dryer operated with electricity.

Finally, the generation of liquid wastes per unit of acrylic acid was the highest for the G-AA (*via* LAC) process, which was attributed to the multiple reaction and separation steps involved in this process, leading to the generation of various liquid waste streams. Subsequently, the G-AA (*via* ACR) process had the second highest liquid wastes per unit of acrylic acid generated during the acrolein separation step as well as due to azeotropic distillation.

3.3. Economic assessment

Fig. 9 presents a comparative analysis of the capital cost components across the four acrylic acid production pathways. When considering the total fixed capital cost, the G-AA (*via* ALY) process exhibited the highest cost ($247.74 million), followed by the G-AA (*via* LAC) ($221.15 million), P-AA (*via* ACR) ($184.49 million), and G-AA (*via* ACR) ($173.63 million) processes. The capital cost of the G-AA (*via* ALY) process was 42% higher than that of the G-AA (*via* ACR) process and 34% higher than that of the conventional P-AA (*via* ACR) process, which can be attributed to the handling and separation processes originated due to the presence of an additional reactant, *i.e.*, formic acid, in the process. The second highest capital cost of the G-AA (*via* LAC) process was due to the complexity of the three-step reaction sequence, involving three reactors, separators, and purification units. Additionally, the solid-handling operations required for the crystallization and filtration of dihydroxyacetone further contribute to the elevated capital investment. Moreover, the G-AA (*via* ACR) process appears to be the least capital-intensive among the four pathways, potentially benefiting from a simpler two-step reaction configuration leading to fewer unit operations and a shorter separation sequence.

Fig. 10 shows the capital investment needed for each unit of the four acrylic acid production processes. For the process having highest capital investment, *i.e.*, the G-AA (*via* LAC) process, the total investment was split nearly evenly between its two units ($168.9 million for unit one and $140.8 million for unit two). The G-AA (*via* LAC) process also showed a relatively balanced distribution across its three units ($100.9 million, $72.8 million, and $102.7 million for unit one, two and three, respectively). In contrast, the G-AA (*via* ACR) and the P-AA (*via* ACR) processes showed a highly uneven distribution, having a higher capital cost for the first units due to the usage of multiple compressors needed to pressurize the reactant stream. To be specific, 61% of the equipment and installation costs needed for unit one of the G-AA (*via* ACR) process and 49% of the equipment and installation costs needed for unit one of the P-AA (*via* ACR) process were contributed by the cost of compressors.

Fig. 11 provides a comprehensive breakdown of the production costs associated with each of the routes examined. It offers valuable insights into the economic feasibility and competitiveness of these processes. It is evident that the raw

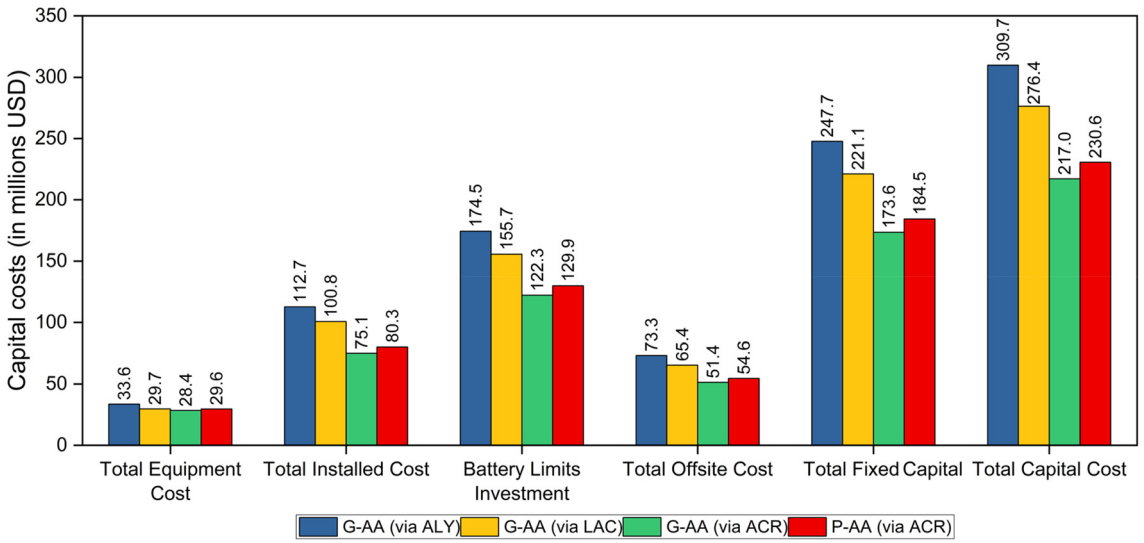

Fig. 9 Capital cost estimation of the four acrylic acid production routes.

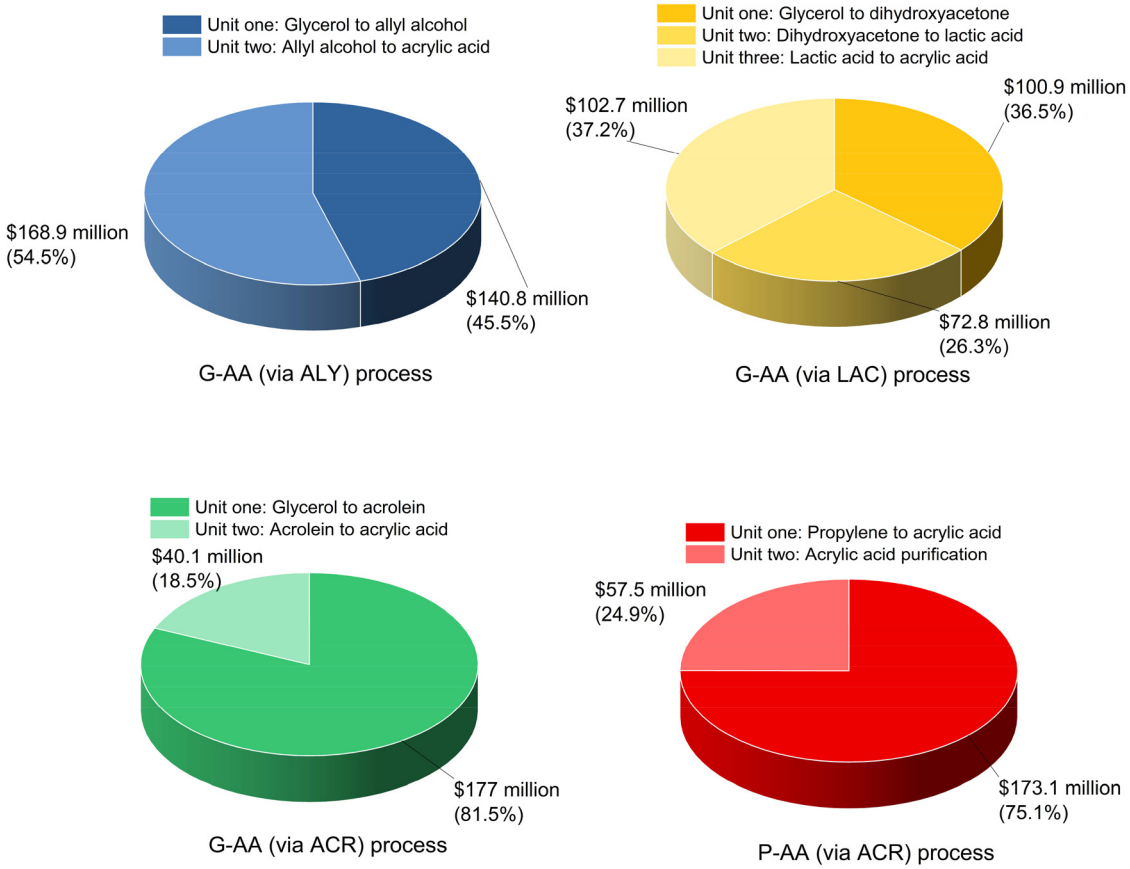

Fig. 10 Distribution of capital investment for each unit of the four acrylic acid production processes.

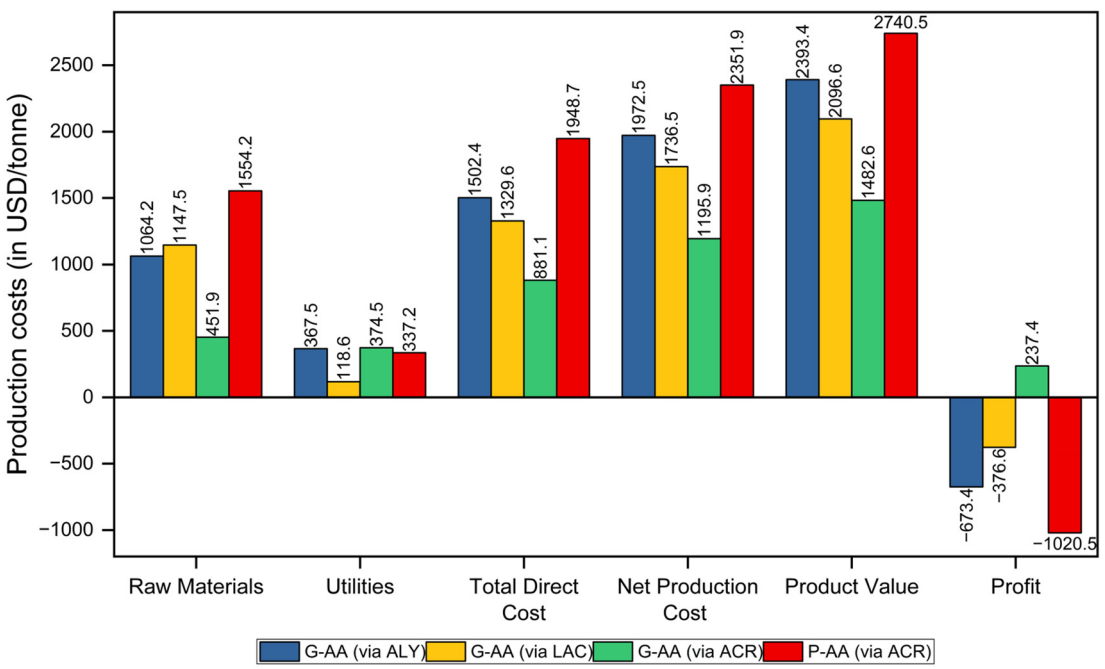

Fig. 11 Production cost estimation of the four acrylic acid production routes.

material costs were the highest for the P-AA (*via* ACR) route (2351.9 USD per tonne). This is expected since propylene is derived from non-renewable fossil fuel sources and is more expensive compared to the cheap glycerol feedstock derived from the biomass. The G-AA (*via* ALY) route had the second highest raw materials (1972.5 USD/tonne) costs and was the highest among the glycerol-based routes due to the requirement of a high amount of formic acid for the first reaction step and DIPE for the liquid–liquid extraction process. The utility costs, which include the expenses for energy (electricity, steam, cooling water and refrigerant), are the highest for the G-AA (*via* ACR) route due to the usage of three compressors in the process, followed by the G-AA (*via* ALY) process.

Overall, the net production cost, which accounts for all the factors such as raw material costs, utilities, plant overhead, taxes, insurances, depreciation, and G&A sales research, was the highest for the P-AA (*via* ACR) route (2351.9 USD per tonne) and G-AA (*via* ALY) route (1972.5 USD per tonne) among the glycerol-based routes, highlighting the potential economic challenges associated with this process. Conversely, the G-AA (*via* ACR) route exhibits the lowest net production cost (1195.9 USD per tonne), suggesting that it is the most economically viable option among the biobased routes. When considering the product value or the minimum selling price of the acrylic acid for the process to be profitable, which represents the cost of producing acrylic acid, the P-AA (*via* ACR) route appears to have the highest value, followed by the G-AA (*via* ALY) and G-AA (*via* LAC) processes, rendering the three processes unprofitable. Fig. 12 shows the contribution of production costs for each unit in the four acrylic acid production processes, where it can be seen that the production costs of unit one are the highest for all the processes except for the G-AA (*via* LAC) process. Moreover, the production costs for unit one of the P-AA (*via* ACR) and G-AA (*via* ALY) processes are greater than the total production costs of the G-AA (*via* ACR) processes. This was mainly caused by most of the production costs for the unit one and could be associated with high-priced raw materials used (*i.e.*, formic acid, DIPE in the case of G-AA (*via* ALY) and propylene in the case of P-AA (*via* ACR)).

Fig. 13 presents a comparison of the annual profitability and payback period across the four different biobased routes

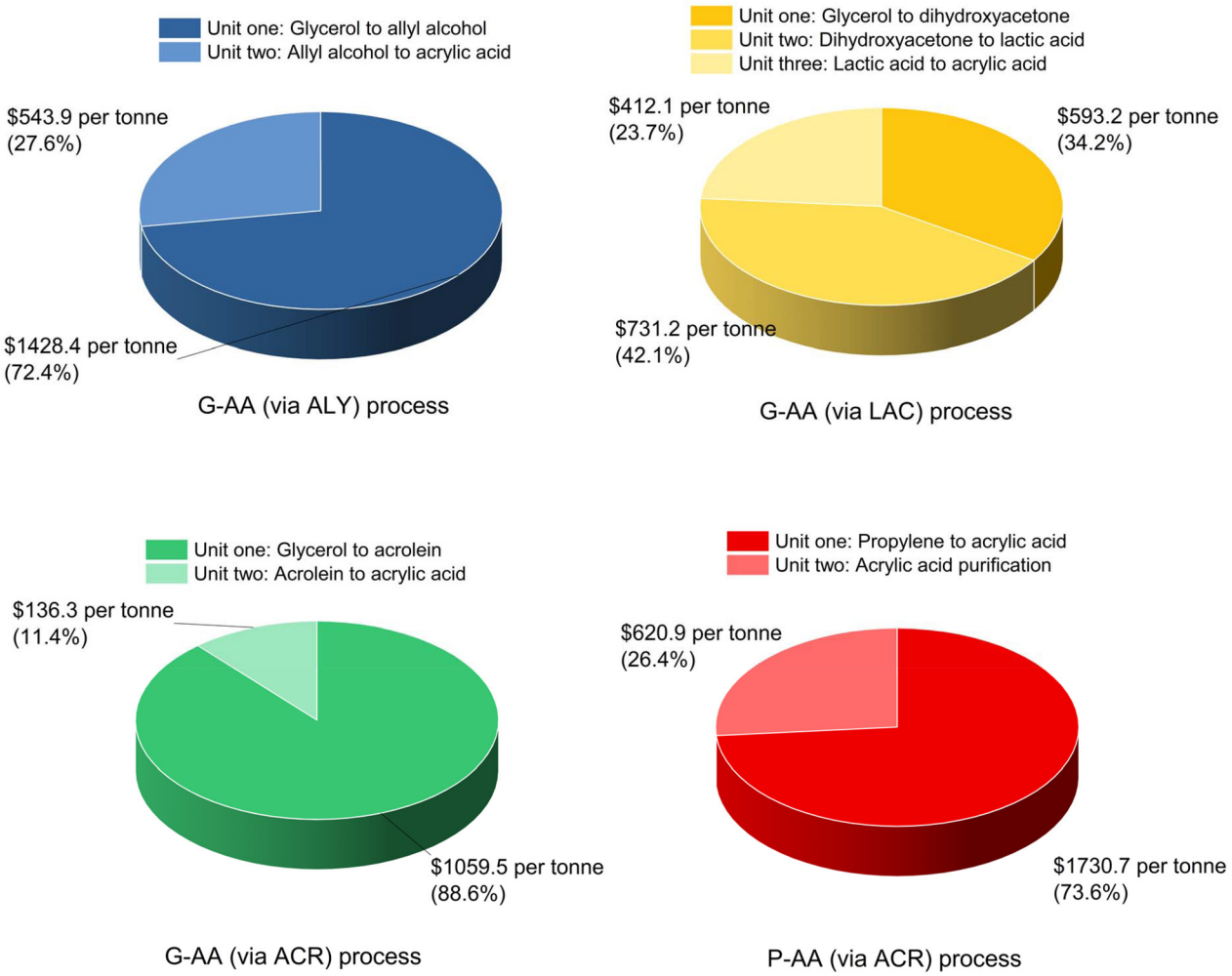

Fig. 12 Distribution of production costs for each unit of the four acrylic acid production processes.

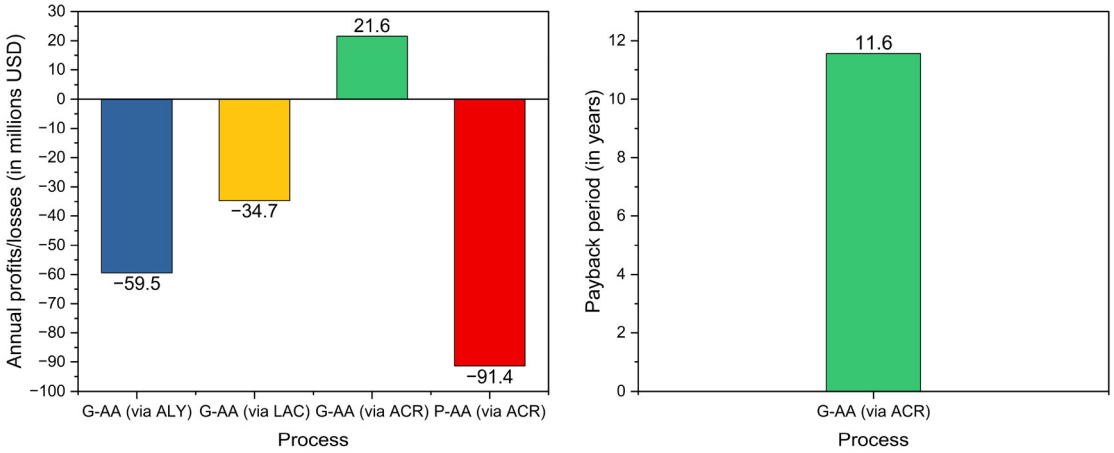

Fig. 13 Annual profits and payback period across the four acrylic acid production routes.

and the conventional propylene-based route for acrylic acid production. While the G-AA (*via* ACR) route showed a positive annual profit of $21.6 million per year, its payback period of 14.3 years (calculated using a 5% discounting factor) was significantly longer than the industry-acceptable range, making it commercially unattractive despite being the best performing among the analysed routes. The other pathways showed even more challenging economics: the G-AA (*via* ALY) route showed substantial annual losses of −$59.5 million per year and the G-AA (*via* LAC) route showed annual losses of −$34.7 million, while the conventional propylene-based P-AA (*via* ACR) route had the largest negative annual profit of −$91.4 million. These negative profits, coupled with the unfavourable payback period even for the best-performing route, suggested that all these processes would require significant technological improvements and cost reductions to become economically viable for industrial implementation.

3.4. Comparison with previous environmental assessments

To evaluate the environmental benefits of the heat integration strategies implemented in this techno-economic study, Fig. 14 compares the global warming potential results from our previous life cycle assessment study[36] with the current work that incorporates heat recovery optimization. The most substantial improvement was observed for the G-AA (*via* ALY) process, where global warming potential decreased from 112 143.70 kg CO_2 eq. per FU in the previous study to 79 747.72 kg CO_2 eq. per FU in the current work with heat integration – representing a 27% reduction in the carbon footprint. Similarly, the G-AA (*via* LAC) process shows improvement from 27% reduction, while the G-AA (*via* ACR) process improved from 69 743.34 to 56 932.88 kg CO_2 eq. per FU (19% reduction). The conventional P-AA (*via* ACR) process demonstrated the smallest improvement, from 55 181.66 to 44 883.11 kg CO_2 eq. per FU (18% reduction). These environmental improvements directly correlate with the energy savings achieved through heat integration (as shown in Fig. 7). The G-AA (*via* ACR) process maintains its position as the most environmentally favourable bio-based

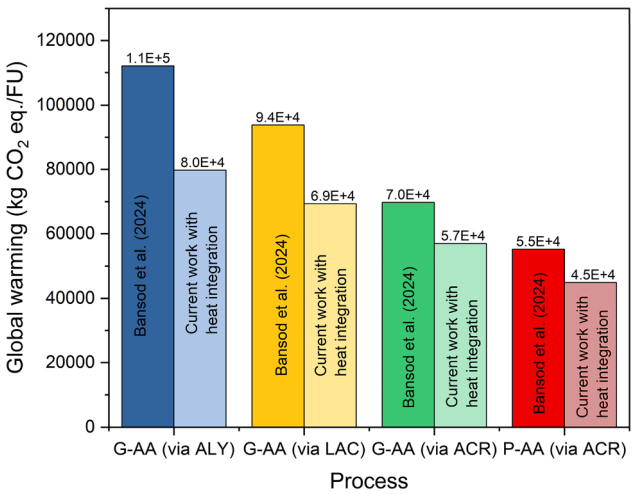

Fig. 14 Comparison of global warming potential between the previous LCA study (Bansod *et al.*, 2024)[36] and the current work with heat integration for the four acrylic acid production processes.

route, with the lowest global warming potential among all glycerol-based alternatives both before and after heat integration. The results demonstrate that economic optimization through heat recovery strategies simultaneously delivers significant environmental benefits. From an environmental perspective, the G-AA (*via* ACR) route represents the most sustainable bio-based alternative to conventional acrylic acid production. However, while this route shows promise from both environmental and technical standpoints, the economic challenges identified in this study, particularly the extended payback period (11.6 years) indicate that further process improvements or favourable market conditions would be needed to achieve commercial viability. Similar environmental improvements were observed across other impact categories through heat integration, with water footprint showing particularly significant reductions (14–48%). More information about other environmental impact categories is provided in Table S27 of the ESI.†

3.5. Sensitivity analysis

The sensitivity analysis of four acrylic acid processes was carried out to investigate the effect of different parameters on annual profits and payback periods. The parameters studied were raw material prices (−75% to 75%), utility prices (−75% to 75%) and acrylic acid prices (−75% to 75%). Fig. 12 presents the effect of changes in the mentioned parameters on the annual profits and payback period for the different acrylic acid production routes. Insights taken from annual profits graphs are also applicable to payback periods; however, an extra crucial metric of the initial capital investment needs to be accounted for. This analysis is crucial in assessing the economic robustness and resilience of these processes under fluc-

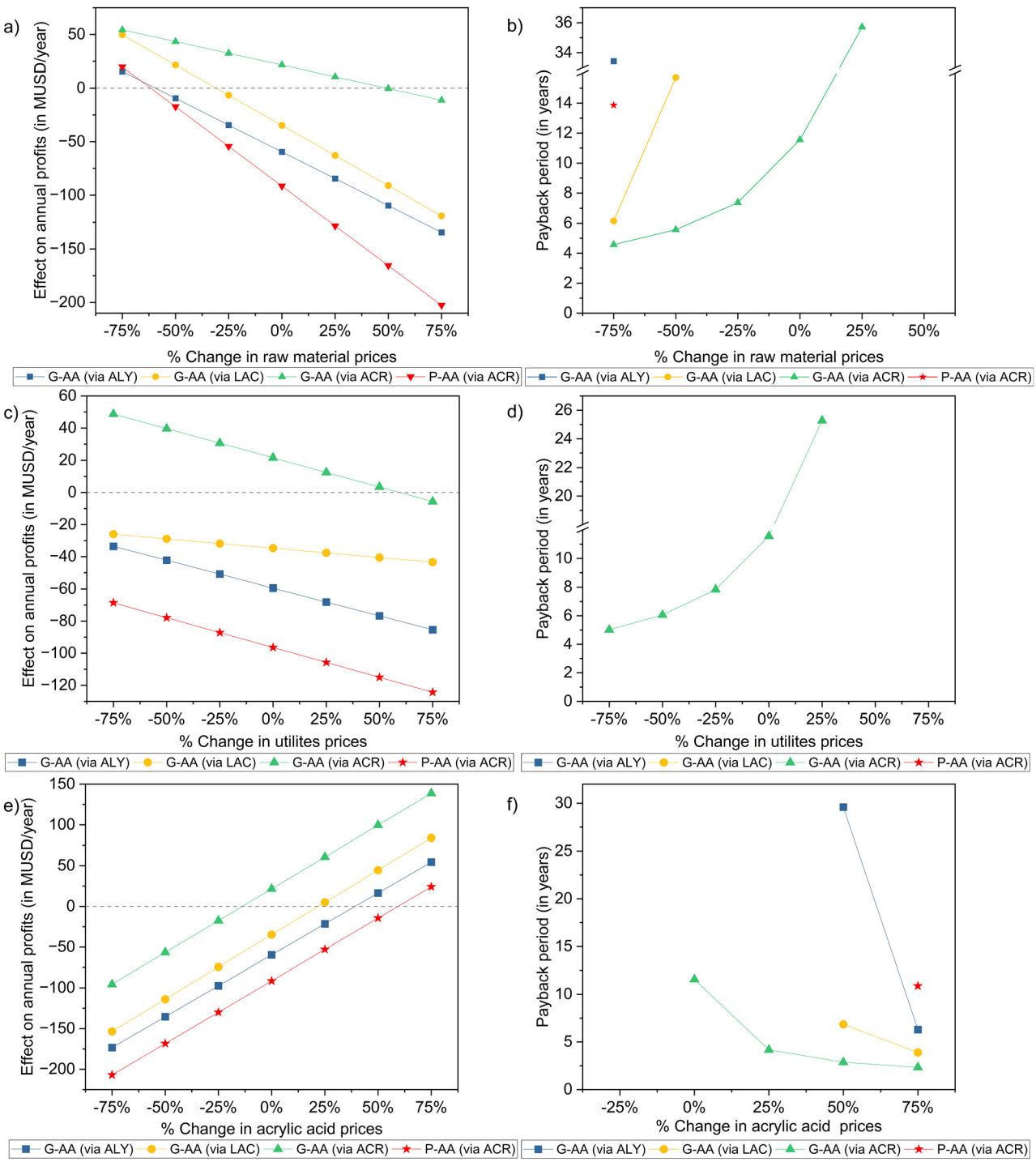

Fig. 15 Sensitivity analysis on the effect of changes in raw material price (a,b), utility price (c,d), and acrylic acid price (e,f) on annual and payback period (b,d,f) for the four acrylic acid production processes.

tuating market conditions and geopolitics. In the case of changing raw material prices, the conventional P-AA (*via* ACR) route showed the highest sensitivity to raw material price changes due to the usage of high-priced propylene in the process. For the bio-based routes, G-AA (*via* ALY) demonstrated significant sensitivity as a result of using formic acid and DIPE, with a 75% decrease in raw material prices pushing annual profits to a profitable value of $15.6 million. The G-AA (*via* ACR) route showed the most resilience, remaining profitable until raw material prices increase by about 25% but with an unfeasible payback period. All processes reached profitability with 75% decrease in raw material prices, with G-AA (*via* ACR) reaching approximately $54.4 million in annual profits at a 75% price reduction (see Fig. 15(a) and (b)).

An analysis of the impact of increased utility prices on the four processes revealed that the G-AA (*via* ACR) route remained profitable even with a 50% price increase, which was understandable as it had the second lowest OER. The other processes showed consistent negative annual profits across all the changes in utility prices, with P-AA (*via* ACR) being most severely impacted, dropping from about −$115.0 million to −$124.3 million as utility prices increase by 75%. The payback period of G-AA (*via* ACR) increased dramatically with rising utility costs, becoming impractical beyond a 25% increase (see Fig. 15(c) and (d)).

The impact of changes in acrylic acid prices on the annual profits and payback period was quite straightforward to comprehend, as can be seen in Fig. 15(e) and (f). Annual profits changed proportionally to the acrylic acid prices for all the processes and a 75% increase in acrylic acid prices made all routes profitable, with G-AA (*via* ACR) achieving the highest profits at around $139 million annually. At the base case scenario of the G-AA (*via* LAC), G-AA (*via* ALY) and P-AA (*via* ACR) routes, the capital investment was not recoverable, but a 50% increase in acrylic acid prices could potentially make the process profitable with a payback period to 6.85 and 29.6 years, respectively. G-AA (*via* ACR) demonstrates the most favourable payback period trend, decreasing to 2.33 years as acrylic acid prices increase by 75% (see Fig. 15(e) and (f)).

4. Conclusions

This study assessed four routes for the production of bio-based acrylic acid, utilizing renewable glycerol feedstock derived from the biodiesel industry.

The economic analysis results showed that the G-AA (*via* ALY) route required the highest capital investment ($247.7 million), followed by the G-AA (*via* LAC) ($221.2 million), P-AA (*via* ACR) ($184.5 million), and G-AA (*via* ACR) ($173.6 million) routes. The G-AA (*via* ACR) route emerged as the only profitable route, with the annual profit of $21.6 million, although with a commercially unattractive payback period of 11.6 years. Moreover, the G-AA (*via* ACR) route had the lowest CO_2 emissions (69 743.34 kg CO_2 eq. per FU), lower overall energy requirement (4.76 kWh $kg_{acrylic\ acid}^{-1}$) and lowest solvent requirement (0.05 $kg_{solvent}$ $kg_{acrylic\ acid}^{-1}$) compared to the glycerol-based routes.

Sensitivity analyses highlighted the importance of raw material and product price fluctuations on the economic viability. The P-AA (*via* ACR) route was the most sensitive to raw material price increases, while the G-AA (*via* ACR) route showed resilience by maintaining profitability until a 25% increase in raw material prices and a 50% increase in utility prices. While the G-AA (*via* ACR) pathway showed considerable promise as a sustainable and economically viable biobased route, there remain opportunities for further research and development to enhance its competitiveness and scalability to improve the payback period of the process. Future opportunities for improvement include process intensification and catalyst optimization to reduce production costs, evaluation of crude glycerol purification impacts, exploration of alternative renewable feedstocks, and integration of renewable energy sources to minimize environmental footprint. Overall, the findings of this study provided valuable insights into the techno-economic feasibility of bio-based acrylic acid production routes, highlighting the potential of glycerol-based pathways as promising alternatives to the conventional fossil fuel-based process.

Author contributions

Yash Bansod: conceptualisation, data curation, investigation, writing – original draft and writing – review and editing; Mostafa Jafari: data curation and investigation; Prashant Pawanipagar: data curation, investigation and writing – review and editing; Kamran Ghasemzadeh: conceptualisation, data curation, investigation and writing – review and editing; Vincenzo Spallina: review, editing, funding acquisition, resources, project administration and supervision; and Carmine D'Agostino: review, editing, funding acquisition, resources, project administration, supervision and validation.

Conflicts of interest

There are no conflicts to declare.

Data availability

The data supporting this article have been included as part of the ESI.†

Acknowledgements

The authors acknowledge the financial support from the EPSRC "Sustainable Production of ACrylic acId from reNewable waste Glycerol" project, EP/V026089/1. Yash Bansod and Prashant Pawanipagar would like to acknowledge the Social Welfare Department, the Government of Maharashtra, India.

References

1 S. Brahma, B. Nath, B. Basumatary, B. Das, P. Saikia, K. Patir and S. Basumatary, *Chem. Eng. J. Adv.*, 2022, **10**, 100284.
2 OECD-FAO Agricultural Outlook 2024–2031, OECD, 2024.
3 A. C. Pinto, L. L. N. Guarieiro, M. J. C. Rezende, N. M. Ribeiro, E. A. Torres, W. A. Lopes, P. A. P. De Pereira and J. B. De Andrade, *J. Braz. Chem. Soc.*, 2005, **16**, 1313–1330.
4 W. N. A. Wan Osman, M. H. Rosli, W. N. A. Mazli and S. Samsuri, *Carbon Capture Sci. Technol.*, 2024, **13**, 100264.
5 P. Verma, M. P. Sharma and G. Dwivedi, *Mater. Today Proc.*, 2018, **5**, 22916–22921.
6 T. Attarbachi, M. D. Kingsley and V. Spallina, *Fuel*, 2023, **340**, 127485.
7 T. Attarbachi, M. Kingsley and V. Spallina, *Ind. Eng. Chem. Res.*, 2024, **63**, 4905–4917.
8 Y. Bansod, K. Ghasemzadeh and C. D'Agostino, *RSC Sustainability*, 2025, **3**, 2605–2618.
9 J. A. Vannucci, M. N. Gatti, N. Cardaci and N. N. Nichio, *Renewable Energy*, 2022, **190**, 540–547.
10 G. Pradhan and Y. C. Sharma, *J. Cleaner Prod.*, 2021, **315**, 127860.
11 A. M. Bruno, C. A. Chagas, M. M. V. M. Souza and R. L. Manfro, *Renewable Energy*, 2018, **118**, 160–171.
12 A. Abdullah, A. Z. Abdullah, M. Ahmed, J. Khan, M. Shahadat, K. Umar and M. A. Alim, *J. Cleaner Prod.*, 2022, **341**, 130876.
13 L. Shen, H. Yin, A. Wang, X. Lu and C. Zhang, *Chem. Eng. J.*, 2014, **244**, 168–177.
14 M.-H. Jo, J.-H. Ju, S.-Y. Heo, C.-B. Son, K. J. Jeong and B.-R. Oh, *Renewable Energy*, 2024, **230**, 120793.
15 D. Liu, B. Dou, H. Zhang, K. Wu, C. Luo, J. Du, D. Xing Gao, H. Chen and Y. Xu, *J. Cleaner Prod.*, 2023, **383**, 135491.
16 V. Singh, S. Arumugam, A. P. Tathod, Kuldeep, B. P. Vempatapu and N. Viswanadham, *Renewable Energy*, 2023, **217**, 119180.
17 R. Li, Z. Wei, H. Li, Z. Yin and Z. Wang, *Renewable Energy*, 2022, **201**, 125–134.
18 G. Li, K. Li, S. Ma and Y. Zhang, *J. Cleaner Prod.*, 2023, **416**, 137988.
19 A. Sandid, V. Spallina and J. Esteban, *Fuel Process. Technol.*, 2024, **253**, 108008.
20 K. K. Ajekwene, *Acrylate polymers for advanced applications*, 2020, pp. 35–46.
21 L. Petrescu, M. Fermeglia and C. C. Cormos, *J. Cleaner Prod.*, 2016, **133**, 294–303.
22 Acrylic Acid Market Outlook, **https://www.futuremarketinsights.com/reports/acrylic-acid-market**, (accessed 11 April 2024).
23 Acrylic Acid Global Market Forecast 2015–2030, **https://www.statista.com/statistics/1245262/acrylic-acid-market-volume-worldwide/**, (accessed 11 April 2024).
24 M. Y. Ahmad, N. I. Basir and A. Z. Abdullah, *J. Ind. Eng. Chem.*, 2021, **93**, 216–227.
25 U. C. Abubakar, Y. Bansod, L. Forster, V. Spallina and C. D'Agostino, *React. Chem. Eng.*, 2023, **8**, 1819–1838.
26 H. Zhao, Y. Jiang, H. Liu, Y. Long, Z. Wang and Z. Hou, *Appl. Catal., B*, 2020, **277**, 119187.
27 V. Canale, L. Tonucci, M. Bressan and N. D'Alessandro, *Catal. Sci. Technol.*, 2014, **4**, 3697–3704.
28 X. Li and Y. Zhang, *ACS Catal.*, 2016, **6**, 143–150.
29 S. C. D'Angelo, A. Dall'Ara, C. Mondelli, J. Pérez-Ramírez and S. Papadokonstantakis, *ACS Sustainable Chem. Eng.*, 2018, **6**, 16563–16572.
30 N. Dhiman, S. R. Yenumala, D. Agrawal, A. Pandey, J. Porwal and B. Sarkar, *Chem. Eng. J.*, 2023, **466**, 143240.
31 X. Zhang, L. Lin, T. Zhang, H. Liu and X. Zhang, *Chem. Eng. J.*, 2016, **284**, 934–941.
32 M. S. Brobbey, J. Louw and J. F. Görgens, *Chem. Eng. Res. Des.*, 2023, **193**, 367–382.
33 O. V. Okoro, L. Nie, H. Alimoradi and A. Shavandi, *Fermentation*, 2022, **8**, 21.
34 S. S. Bhagwat, Y. Li, Y. R. Cortés-Peña, E. C. Brace, T. A. Martin, H. Zhao and J. S. Guest, *ACS Sustainable Chem. Eng.*, 2021, **9**, 16659–16669.
35 A. Sandid, J. Esteban, C. D'Agostino and V. Spallina, *J. Cleaner Prod.*, 2023, **418**, 138127.
36 Y. Bansod, P. Pawanipagar, K. Ghasemzadeh and C. D'Agostino, *Green Chem.*, 2024, **26**, 9840–9858.
37 A. C. Dimian, C. S. Bildea and A. A. Kiss, *Applications in Design and Simulation of Sustainable Chemical Processes*, 2019, pp. 521–569.
38 M. E. T. Alvarez, E. B. Moraes, A. B. Machado, R. Maciel Filho and M. R. Wolf-Maciel, *Applied Biochemistry and Biotecnology*, 2007, pp. 451–461.
39 A. C. Dimian, C. S. Bildea and A. A. Kiss, *Applications in Design and Simulation of Sustainable Chemical Processes*, 2019, pp. 521–569.
40 T. Ohara, T. Sato, N. Shimizu, G. Prescher, H. Schwind, O. Weiberg, K. Marten, H. Greim, T. D. Shaffer and P. Nandi, *Ullmann's Encyclopedia of Industrial Chemistry*, 2020, pp. 1–21.
41 Statista, UK Biodiesel Production, 2024, **https://www.statista.com/statistics/791692/biodiesel-production-united-kingdom-uk/**, (accessed 30 September 2024).
42 G. Towler and R. Sinnott, *Chemical engineering design: principles, practice and economics of plant and process design*, Butterworth-Heinemann, 2021.
43 A. Sandid, J. Esteban, C. D'Agostino and V. Spallina, *J. Cleaner Prod.*, 2023, **418**, 138127.
44 M. S. Peters and K. D. Timmerhaus, *Plant design and economics for chemical engineers*, McGraw-Hill International, 2018.
45 N. Wörz, A. Brandner and P. Claus, *J. Phys. Chem. C*, 2010, **114**, 1164–1172.
46 Oleoline Quarterly Glycerine Market Report, **https://www.oleoline.com/products/Quarterly-Glycerine-Market-Report-3.html**, (accessed 30 September 2024).
47 K. C. Premlall and D. Lokhat, *Energies*, 2020, **13**, 1971.

48 Y. Zhu, D. Youssef, C. Porte, A. Rannou, M. P. Delplancke-Ogletree and B. L. Mi Lung-Somarriba, *J. Cryst. Growth*, 2003, **257**, 370–377.
49 M. R. Ebersole, *J. Phys. Chem.*, 2002, **5**, 239–255.
50 Towering Skills Cost Indices, **https://toweringskills.com/financial-analysis/cost-indices/**, (accessed 12 April 2024).
51 Intratec Plant Location Factors, **https://www.intratec.us/products/plant-location-factors**, (accessed 12 April 2024).
52 A. H. Tseng and B. Y. Yu, *Process Saf. Environ. Prot.*, 2024, **191**, 983–994.
53 ChemAnalyst, Formic Acid Prices, **https://www.chemanalyst.com/Pricing-data/formic-acid-1242**, (accessed 12 April 2024).
54 IndexBox, Acetone Price, **https://www.indexbox.io/search/acetone-price-the-uk/**, (accessed 12 April 2024).
55 Pricing - Methanex|Methanex, **https://www.methanex.com/about-methanol/pricing/**, (accessed 7 November 2024).
56 ChemAnalyst, Diisopropyl Ether, **https://www.chemanalyst.com/Pricing-data/diisopropyl-ether-1137**, (accessed 12 April 2024).
57 ChemAnalyst, Toluene Price, **https://www.chemanalyst.com/Pricing-data/toluene-30**, (accessed 12 April 2024).
58 ChemAnalyst, Propylene Prices, **https://www.chemanalyst.com/Pricing-data/propylene-51**, (accessed 12 April 2024).
59 D. Brennan, *Process industry economics: principles, concepts and applications*, Elsevier, 2020.
60 ChemAnalyst, Acrylic Acid Prices, **https://www.chemanalyst.com/Pricing-data/acrylic-acid-20**, (accessed 12 April 2024).
61 Prices of fuels purchased by manufacturing industry, UK Government, **https://www.gov.uk/government/statistical-data-sets/prices-of-fuels-purchased-by-manufacturing-industry**, (accessed 12 April 2024).
62 J. Wu, D. Xu, P. Shi, J. Gao, L. Zhang, Y. Ma and Y. Wang, *J. Chem. Thermodyn.*, 2018, **118**, 139–146.
63 CDC - NIOSH Pocket Guide to Chemical Hazards - Allyl alcohol, **https://www.cdc.gov/niosh/npg/npgd0017.html**, (accessed 7 November 2024).
64 S. Goto, *Chem. Eng. Trans.*, 2019, **77**, 709.
65 L. Mo, J. Shao-Tong, P. Li-Jun, Z. Zhi and L. Shui-Zhong, *Chem. Eng. Res. Des.*, 2011, **89**, 2199–2206.
66 B. Yan, Z. H. Liu, Y. Liang and B. Q. Xu, *Ind. Eng. Chem. Res.*, 2020, **59**, 17417–17428.
67 CDC - NIOSH Pocket Guide to Chemical Hazards - Acrolein, **https://www.cdc.gov/niosh/npg/npgd0011.html**, (accessed 7 November 2024).
68 W. L. Luyben, *Comput. Chem. Eng.*, 2016, **93**, 118–127.